

**Design, Synthesis, Physicochemical and Pharmacological
Profiling of 7-Hydroxy-5-oxopyrazolo[4,3-b]pyridine-6-
carboxamide Derivatives with Anti-Osteoarthritic Activity in Vivo**

Claudia Mugnaini, Magdalena Kostrzewa, Marta Bryk, Ali Mokhtar Mahmoud, Antonella Brizzi, Stefania Lamponi, Gianluca Giorgi, Francesca Ferlenghi, Federica Vacondio, Paola Maccioni, Giancarlo Colombo, Marco Mor, Katarzyna Starowicz, Vincenzo Di Marzo, Alessia Ligresti, and Federico Corelli
J. Med. Chem., **Just Accepted Manuscript** • DOI: 10.1021/acs.jmedchem.0c00595 • Publication Date (Web): 09 Jun 2020

Downloaded from pubs.acs.org on June 10, 2020

Just Accepted

"Just Accepted" manuscripts have been peer-reviewed and accepted for publication. They are posted online prior to technical editing, formatting for publication and author proofing. The American Chemical Society provides "Just Accepted" as a service to the research community to expedite the dissemination of scientific material as soon as possible after acceptance. "Just Accepted" manuscripts appear in full in PDF format accompanied by an HTML abstract. "Just Accepted" manuscripts have been fully peer reviewed, but should not be considered the official version of record. They are citable by the Digital Object Identifier (DOI®). "Just Accepted" is an optional service offered to authors. Therefore, the "Just Accepted" Web site may not include all articles that will be published in the journal. After a manuscript is technically edited and formatted, it will be removed from the "Just Accepted" Web site and published as an ASAP article. Note that technical editing may introduce minor changes to the manuscript text and/or graphics which could affect content, and all legal disclaimers and ethical guidelines that apply to the journal pertain. ACS cannot be held responsible for errors or consequences arising from the use of information contained in these "Just Accepted" manuscripts.

Design, Synthesis, Physicochemical and Pharmacological Profiling of 7-Hydroxy-5-oxopyrazolo[4,3-*b*]pyridine-6-carboxamide Derivatives with Anti-Osteoarthritic Activity in Vivo

Claudia Mugnaini,^{†,¶,*} Magdalena Kostrzewa,^{‡,#,¶} Marta Bryk,[§] Ali Mokhtar Mahmoud,[‡] Antonella Brizzi,[†] Stefania Lamponi,[†] Gianluca Giorgi,[†] Francesca Ferlenghi,^{||} Federica Vacondio,^{||} Paola Maccioni,[⊥] Giancarlo Colombo,[⊥] Marco Mor,^{||} Katarzyna Starowicz,[§] Vincenzo Di Marzo,[‡] Alessia Ligresti,^{‡,*} and Federico Corelli[†]

[†]*Department of Biotechnology, Chemistry and Pharmacy, University of Siena, Via Aldo Moro 2, 53100 Siena, Italy*

[‡]*Endocannabinoid Research Group, Institute of Biomolecular Chemistry, National Research Council of Italy, Via Campi Flegrei 34, 80078 Pozzuoli (Napoli), Italy*

[#]*Institute of Genetics and Biophysics, National Research Council of Italy, Via Pietro Castellino 111, 80131 Napoli, Italy*

[§]*Department of Neurochemistry, Institute of Pharmacology, Polish Academy of Sciences, ul. Smetna 12, 31-343 Cracow, Poland*

^{||}*Department of Food and Drug, University of Parma, Parco Area delle Scienze 27/A, 43124 Parma, Italy*

[⊥]*Institute of Neuroscience, National Research Council of Italy, S.S. 554, km 4,500, 09042 Monserrato (Cagliari), Italy*

ABSTRACT

The hallmark of joint diseases, such as osteoarthritis (OA), is pain, originating from both inflammatory and neuropathic components, and compounds able to modulate the signal transduction pathways of the cannabinoid type-2 receptor (CB2R) can represent a helpful option in the treatment of OA. In this perspective, a set of 18 cannabinoid type-2 receptor (CB2R) ligands was developed based on an unprecedented structure. With the aim of improving the physicochemical properties of previously reported 4-hydroxy-2-quinolone-3-carboxamides, a structural optimization program led to the discovery of isosteric 7-hydroxy-5-oxopyrazolo[4,3-*b*]pyridine-6-carboxamide derivatives. These new compounds are endowed with high affinity for the CB2R and moderate to good selectivity over the cannabinoid type-1 receptor (CB1R), associated with good physicochemical characteristics. As to the functional activity at the CB2R, compounds able to act either as agonists or inverse agonists/antagonists were discovered. Among them, compound **51** emerged as a potent CB2R agonist able to reduce pain in rats carrying OA induced by injection of monoiodoacetic acid (MIA).

Keywords

CB2 receptor

CB2-Selective ligands

Osteoarthritis

Pain

Isosterism

INTRODUCTION

Painful and disabling pathologies shared by most of the people worldwide include rheumatic and joint diseases,¹ whose prevalence is expected to rise mainly because the world population grows older and medical advances lengthen life expectancy. Osteoarthritis (OA), a prevalent disease accompanied by chronic, debilitating pain, is the most common form of arthritis and a leading cause of disability for older individuals in developed countries,² where the increasingly higher incidence of obesity is an important factor besides ageing. It is estimated that 25% of individuals affected by osteoarthritis are prevented from performing daily activities.³ OA-induced pain is related to activation and release of local pro-inflammatory mediators and is accompanied by the destruction of tissue. However, clinically there is often disparity between the degree of pain perception and the extent of joint changes in subjects with OA.⁴

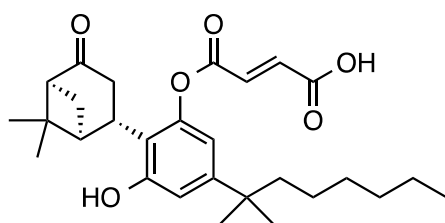
Nowadays, a growing body of evidence shows that the development of damage to joints and bones, as well as joint-related functional impairment, involve both local and, even more, systemic inflammation.⁵ The hallmark symptom of joint diseases is pain,⁶ which originates from both inflammatory and neuropathic components, the latter seemingly being the major determinant of the intensity and quality of pain, although specific nerve lesions have not yet been identified in these pathologies.⁶ Whilst it is well established that osteoarthritis is a heterogeneous condition with a variety of pathophysiologic drivers leading to multiple phenotypes,⁷ the pathogenesis of this disease is an intricate multifactorial process not fully clarified yet. In this scenario, the existence of a robust cross-talk between cartilage and subchondral bone as well as the occurrence of alterations of all junction structures (cartilage, bone, synovium, matrix, nerve endings, and blood vessels) is widely recognized.⁸ In joint diseases, dysregulation and persistent activation of mast cells play a role at different levels, by altering the balance between cartilage and subchondral bone, promoting degenerative processes, and favoring the development of spinal neuroinflammation.⁹ Among the inflammatory mediators involved in this pathological mechanism, interleukin- (IL-) 1 β has been recognized as an important initiator of OA pathophysiological development.¹⁰

The therapeutic options currently available for treatment of osteoarthritis remain limited.¹¹ The traditional pharmacological intervention addressing chronic pain in this condition basically relies on symptomatic use of paracetamol and nonsteroidal anti-inflammatory drugs. There is an urgent need for effective osteoarthritis pharmacotherapy, able to prevent joint degeneration, to delay disease progression, and to restore the organ functionality in affected individuals.¹² Accordingly, a convincing approach to address effectively this problem focuses on the development of disease-modifying drugs, and compounds targeting cannabinoid receptors and peroxisome proliferator-activated receptors (PPARs) represent a potential answer to this therapeutic need.⁹

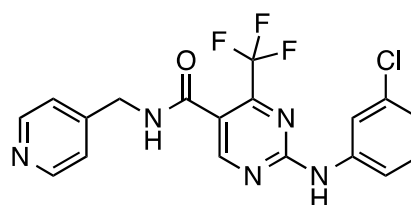
Type-1 cannabinoid receptors (CB1R) and type-2 cannabinoid receptors (CB2R) are the main receptors of the endocannabinoid system that have been identified so far.¹³ Given their wide distribution in the body, these CBRs are implicated in several physiological and pathological processes and can be regarded as intriguing targets for potential pharmacotherapies in a number of disorders.¹⁴ In this context, CBRs draw special attention, as they play a key role in bone formation, resorption, and growth. In particular, both CBRs are present in the skeleton, with CB1R expressed on nerve endings, whereas CB2R is found in osteoblasts, osteocytes, and osteoclasts.^{15,16} Under pathological conditions, hypertrophic chondrocytes express both receptors,¹⁷ while synovial tissue fibroblasts of individuals affected by rheumatoid arthritis¹⁸ and immune system cells like mast cells mainly express CB2R. Both CB1 and CB2 receptor agonists play a protective role in joint diseases, as these receptors are involved in age-related bone remodeling and bone loss; in addition, due to its localization on cells of the immune system, the CB2R mediates immunomodulatory and anti-inflammatory effects as well. As a result, the development of CB2R agonists, which are devoid of the unwanted psychotropic effects ensuing from CB1R activation in the central nervous system (CNS), may be a promising avenue to novel, disease-modifying drug candidates for the treatment of the osteoarthritis process and chronic pain.¹⁹ Accordingly, many efforts were made by academic and industrial laboratories to identify novel CB2R selective agonists because of their therapeutic potential

in the treatment of a number of pathological conditions, such as neurodegenerative diseases, pain, ischemic stroke, inflammation, autoimmune diseases, osteoporosis, and cancer.²⁰ As a result of this endeavor, a significant number of CB2R agonists with even excellent in vitro activities have been discovered, and some of them have successfully passed the preclinical evaluation to enter clinical trials (selected examples are reported in Chart 1),^{19,20a} also by virtue of balanced physicochemical properties and favorable pharmacokinetic characteristics.

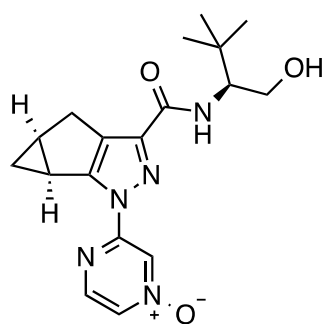
Chart 1. Selected CB2 Agonists in Clinical Development



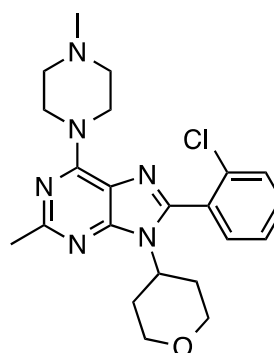
PRS-211375 (Cannabinor)



GW833972



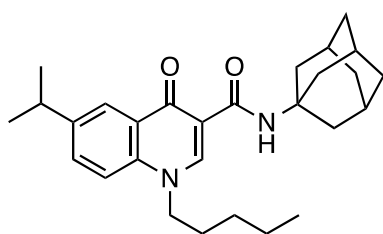
APD371 (Olorinab)



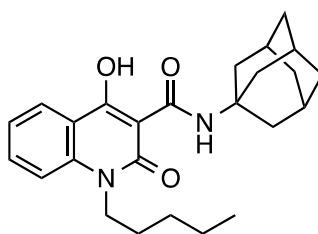
LY2828360

During the last decade, we have been actively investigating new cannabinoid ligands based on the quinolone scaffold and our endeavor has led to the discovery of several compounds (e.g. **1**, Chart 2) showing remarkable affinity and selectivity at CB2R.²¹

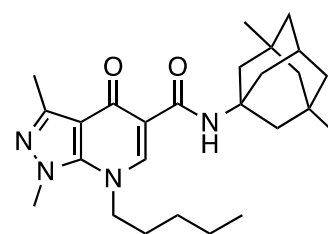
Chart 2. Representative Examples of Quinolones as Potent and Selective CB2R Ligands



1 (COR167)
 $K_{iCB_2} = 6.3$ nM
 $K_{iCB_1} = 1,220$ nM
 SI = 194



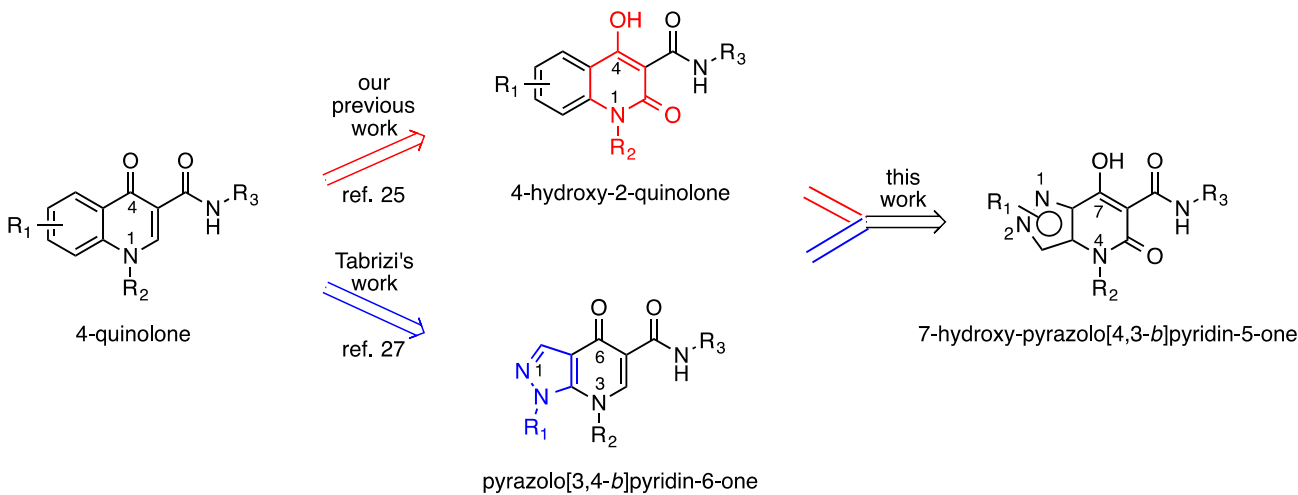
2
 $K_{iCB_2} = 0.97$ nM
 $K_{iCB_1} = 108$ nM
 SI = 112



3
 $K_{iCB_2} = 9.83$ nM
 $K_{iCB_1} = 1,050$ nM
 SI = 107

Compound **1** (usually referred to as COR167) behaved as a full agonist and was further assayed in in vitro, ex vivo, and in vivo tests, where it displayed: *i*) potent immunomodulatory activity on immune cells from healthy subjects and patients with multiple sclerosis,²² *ii*) protective effects on rat brain tissues toward ischemia and reperfusion-induced injury,²³ and *iii*) anti-nociceptive properties,²⁴ thereby validating CB2R as a therapeutic target and becoming a useful pharmacological tool for further investigations. Very recently, we and other groups have introduced significant modifications to the quinolone scaffold of CB2R ligands aimed at improving their general physicochemical properties. Thus, on the one hand, our approach relied on the modification of the 4-quinolones into 4-hydroxy-2-quinolones,²⁵ such as compound **2**, in order to get slightly acidic compounds with pKa values typically in the range 4.2-5.0²⁶ and hence expected to show better aqueous solubility at physiological pH. On the other hand, Aghazadeh Tabrizi *et al.* opted for a scaffold hopping strategy, by replacing the benzene ring of 4-quinolones with pyrazole, giving rise to two isomeric series, namely pyrazolo[3,4-*b*]pyridine-5-carboxamides (e.g. **3**, Chart 2),²⁷ and pyrazolo[1,5-*a*]pyrimidine-6-carboxamides.²⁸ Both works led to some advances in terms of physicochemical optimization of the target cannabinoid ligands, associated with preservation of binding affinity and receptor selectivity. As a further attempt to improve the hydrophilic/lipophilic balance of CB2R ligands, we conceived a more marked structural modification of the original 4-quinolone nucleus, stemming from the combination of both approaches mentioned above and leading to molecules based on the new scaffold 7-hydroxy-5-oxopyrazolo[4,3-*b*]pyridin-6-carboxamide (Chart 3).

Chart 3. Design of Novel 7-Hydroxypyrazolo[4,3-*b*]pyridine-5-one Derivatives

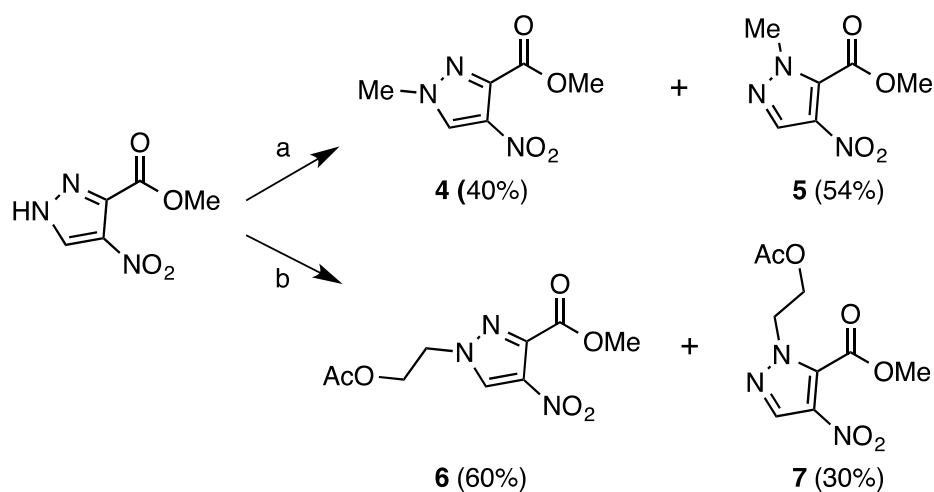


Here, we describe the synthesis, drug-like and physicochemical properties, and in vitro pharmacological profiling of novel CB2R selective ligands, as well as the in vivo evaluation of a selected CB2R agonist in a rat model of osteoarthritis.

RESULTS AND DISCUSSION

Chemistry. The chemical synthesis to attain the target pyrazolo[4,3-*b*]pyridine derivatives started with the alkylation of commercially available methyl 4-nitro-1*H*-pyrazole-3-carboxylate (Scheme 1) with either iodomethane or 2-bromoethyl acetate to introduce a first element of chemical diversity into the final compounds.

Scheme 1^a

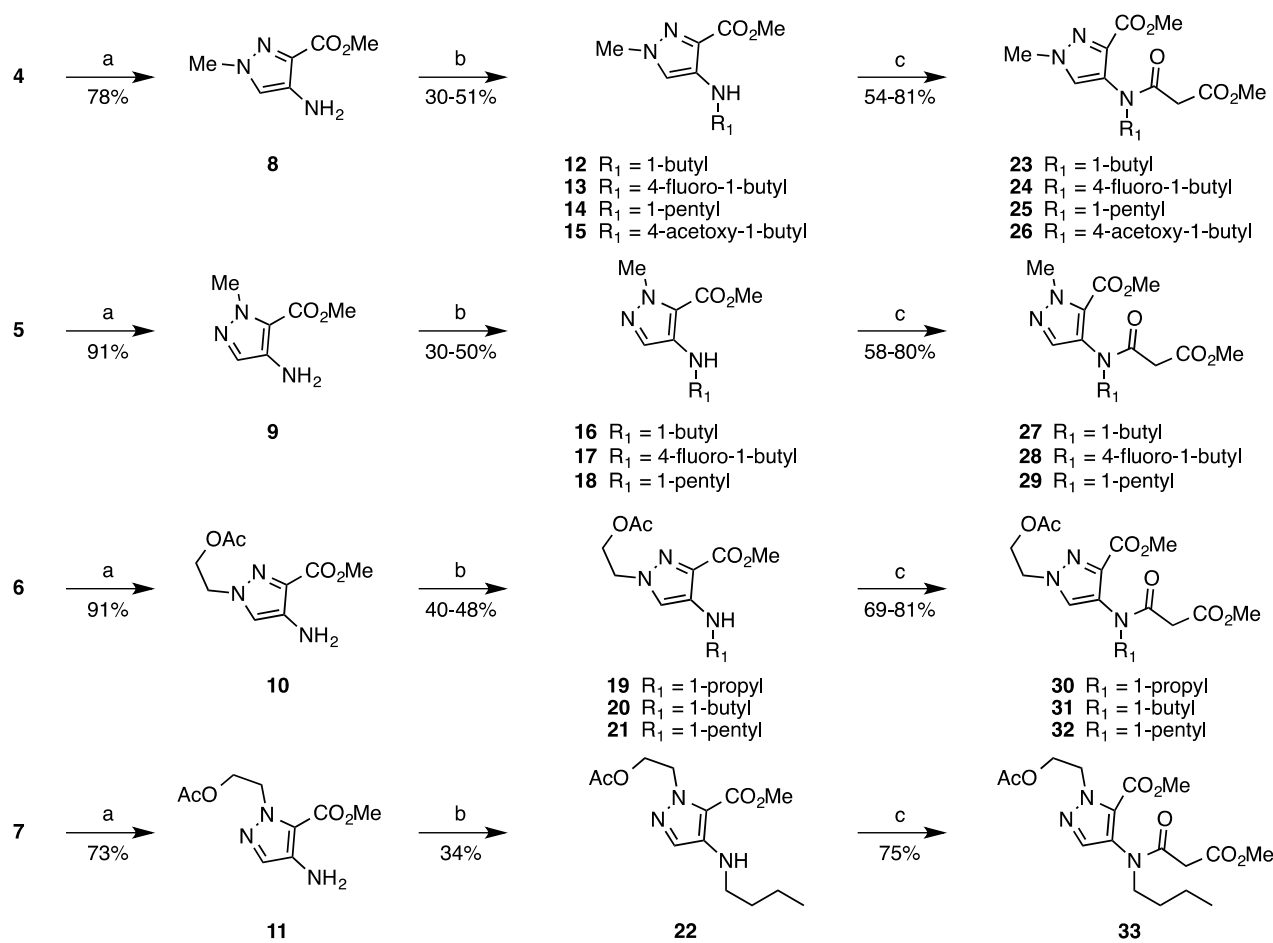


^aReagents and conditions: (a) CH_3I , K_2CO_3 , acetone, 50°C , 2 h; (b) 2-bromoethyl acetate, KI , K_2CO_3 , acetone, 50°C , 24 h

Both reactions produced a mixture of regioisomers **4/5** and **6/7** which were separated by column chromatography on silica gel. Their structure was assigned by X-ray crystallographic analysis (see Supporting Information), that unambiguously showed as in both cases the more polar isomers were **4** and **6**, alkylated at the 2-position, while the faster eluting isomers **5** and **7** were 1-substituted pyrazole derivatives. Regioisomers **4** and **6** were also obtained in slightly higher percentage (**4:5** = 1.3:1 and **6:7** = 2:1).

Compounds **4-7** were the precursors of four different series of pyrazolo[4,3-*b*]pyridine derivatives (Scheme 2).

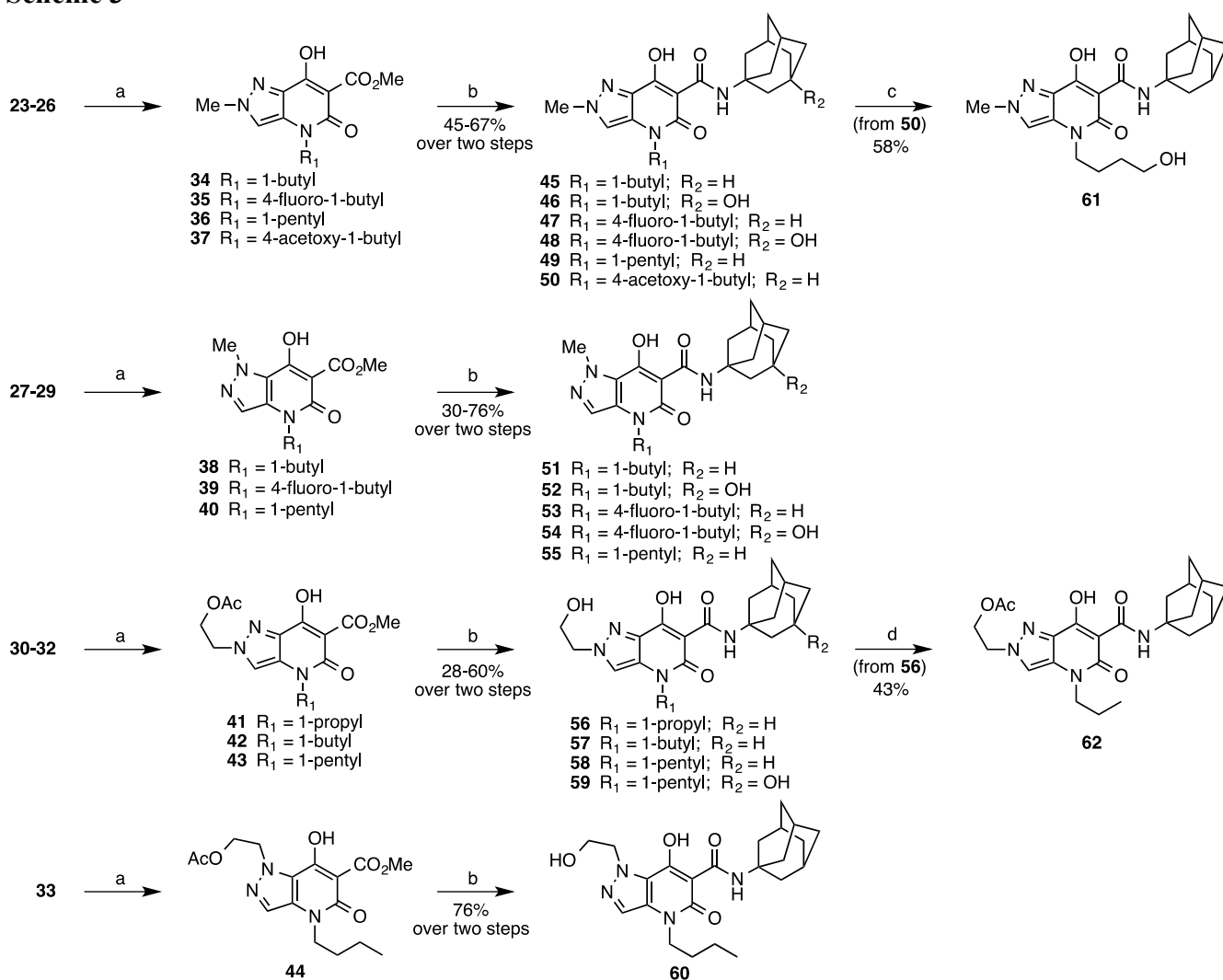
Scheme 2^a



“Reagents and conditions: (a) Fe, CaCl₂, EtOH, H₂O, 60 °C, 3 h; (b) appropriate alkyl iodide or bromide, dry DMF, 50 °C, 6-8 h; (c) 3-chloro-3-oxopropionate, NEt₃, dry DCM, rt, 2 h.

Reduction of the nitro group was accomplished using Fe/CaCl₂ in ethanol/water and amines **8-11** were subjected to alkylation with different haloalkyl derivatives. This reaction was best performed in DMF as solvent and in the absence of any added base to prevent the formation of products doubly substituted on the amino group, likely due to higher nucleophilic reactivity of secondary amines compared to primary ones. Being also the most basic species present in solution, the initially formed monoalkylated compounds preferentially acted as scavenger for produced HX, making possible the selective conversion of the primary amines **8-11** into the corresponding secondary amines **12-22**. After all, this procedure allowed to obtain the expected compounds **12-22** as the main reaction products, albeit in only moderate yield (30-44% after chromatographic purification), as well as to enhance their chemical diversity. Subsequent acylation of secondary amines **12-22** with methyl 3-

chloro-3-oxopropionate led to the corresponding amides **23-33**, which in turn were subjected to Dieckmann condensation (Scheme 3) under classical conditions (NaH/cat. MeOH/THF) to give the pyrazolo[4,3-*b*]pyridine esters **34-44**.

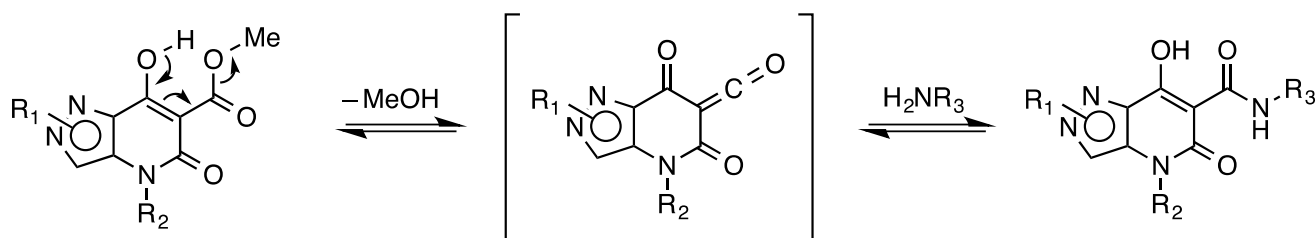
Scheme 3^a

^aReagents and conditions: (a) NaH, MeOH (cat.), dry THF, 60 °C, 2 h; (b) 1-aminoadamantane or 3-aminoadamantan-1-ol, THF, toluene, reflux, 1-2 h; (c) 10% NaOH, H₂O, reflux, 1 h; (d) AcCl, NEt₃, dry DCM, rt, 2.5 h.

Due to their remarkable polarity and very low solubility in most organic solvents, these compounds were directly used in the next reaction. Treatment of **34-44** with 1-adamantylamine or 3-amino-1-

adamantanol in refluxing toluene, with azeotropic removal of formed methanol, provided in good yield the final adamantylamides **45-60**, which could be easily purified by chromatography and/or crystallization. This unexpectedly fast and high-yielding conversion of the ester group into an amide functionality without using specific catalysts can be rationalized by taking into account an elimination-addition equilibrium, leading to the formation of a highly electrophilic ketene intermediate, with the azeotropic removal of methanol driving the reaction to completion (Scheme 4), as already reported by Jansson *et al.* for similar substrates.²⁹

Scheme 4.



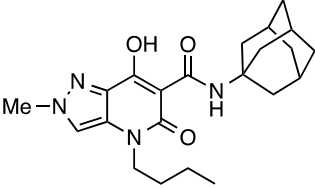
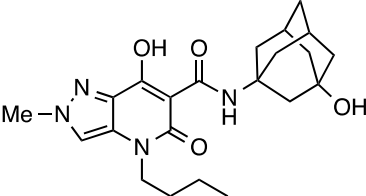
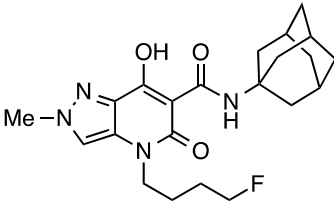
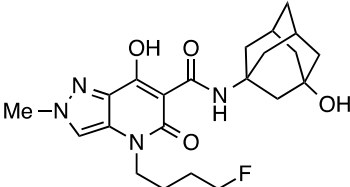
Interestingly enough, during this reaction, diesters **41-44** underwent concurrent deacetylation on the pyrazole side chain so as to yield directly the final compounds **56-60**. Conversely, the acetoxy moiety of **37** outlasted those reaction conditions and provided a still acetylated compound **50**, that was then converted into **61** by basic hydrolysis. On the other hand, deacetylated compound **56** was reacylated to **62** in order to evaluate the influence of this structural modification on receptor binding affinity in *in vitro* assays.

All the final compounds were characterized by MS, ¹H NMR, and ¹³C NMR. In particular, ¹H NMR spectra revealed the presence of double signals, as shown as an example by ¹H NMR spectrum of compound **51** (Supporting Information). The interested signals are those concerning N1 methyl, C3-H, amide NH, and enolic OH, while the alkyl side chain at N4 position and adamantane moiety do not give rise to double signals. This outcome may account for possible tautomeric equilibria in solution, such as that highlighted in Figure 1S (Supporting Information) which involves two most

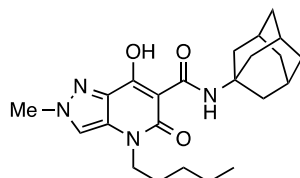
likely tautomers, although we cannot rule out the possibility that other tautomeric forms might be present as well. Based on the ^1H NMR spectra registered in CDCl_3 , we were able to estimate the ratio between tautomers present in solution for the four families of final amides, which resulted to be roughly 99:1 for **45**, 3:1 for **51**, 8:1 for **57**, and 1.3:1 for **60**.

Affinity/Selectivity for Cannabinoid Receptors and Functional Activity. The binding affinities (K_i values) of compounds **45-62** for human recombinant CB1R and CB2R are reported in Table 1.

Table 1. CB1R and CB2R Affinity Values for Compounds 45-62 in Comparison with the Selective CB2R Ligand SR144528.^{a,b}

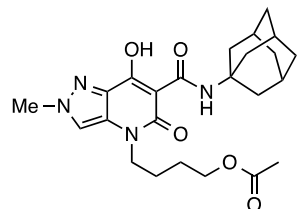
Compd	Structure	CB1R ^c	CB2R ^d	SI ^e
		K_i^f (nM)	K_i^f (nM)	
45		231 ± 76	2.5 ± 0.2	92
46		$>1,000$	10.6 ± 1.1	>94
47		532 ± 8	2.1 ± 0.2	253
48		$>1,000$	6.2 ± 0.1	>161

49

 33.5 ± 0.9 0.18 ± 0.01

167

50

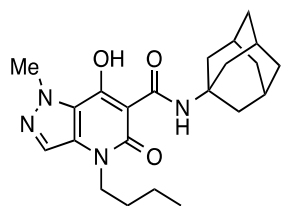


>1,000

 17.3 ± 3.9

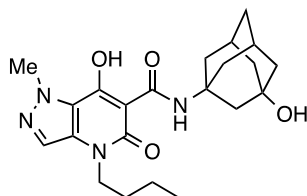
>57

51

 69.0 ± 3.3 1.8 ± 0.4

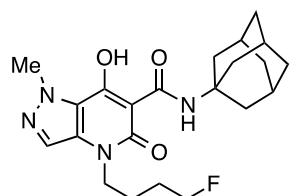
38

52

 86.9 ± 14.9 19.3 ± 0.6

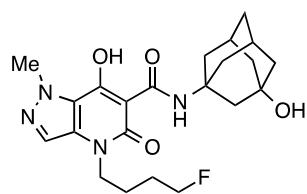
4

53

 39.3 ± 0.8 1.4 ± 0.2

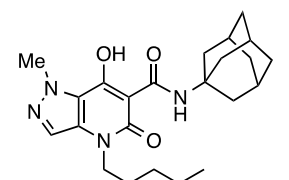
28

54

 161 ± 55 18.9 ± 0.8

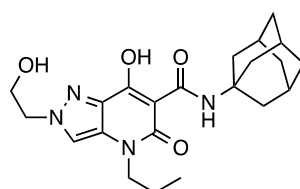
8

55

 56.0 ± 15.8 0.90 ± 0.01

62

56



> 1,000

 159 ± 13

6

57		>1,000	18.4 ± 1.9	>54
58		108 ± 8	4.8 ± 0.7	22
59		492 ± 40	57.1 ± 2.3	9
60		>1,000	27.1 ± 2.9	>37
61		> 1,000	14.3 ± 0.8	>70
62		>1,000	186 ± 18	5
SR144528 ^{g,h}		116 ± 22	1.8 ± 0.5	64

^aData represent mean values ± SD for at least three separate experiments performed in duplicate and are expressed as K_i (nM). ^bFor both receptor binding assays, the new compounds were tested using membranes from HEK cells transfected with either CB1R or CB2R and [³H]-(-)-*cis*-3-[2-hydroxy-4-

(1,1-dimethylheptyl)phenyl]-*trans*-4-(3-hydroxypropyl)cyclohexanol ([³H]CP-55,940). ^cCB1R: human cannabinoid type 1 receptor. ^dCB2R: human cannabinoid type 2 receptor. ^eSI: selectivity index for CB2R, calculated as $K_i(\text{CB1R})/K_i(\text{CB2R})$ ratio. ^f K_i : inhibitor constant, that is, the concentration of the competing ligand that will bind to half the binding sites at equilibrium in the absence of radioligand or other competitors. ^gCB2 reference compound. ^hThe binding affinities of reference compounds were evaluated in parallel with test compounds under the same conditions.

The compounds were evaluated in parallel with compound SR144528³⁰ as reference CB2R ligand, as previously described.²¹ All eighteen compounds tested displayed significant binding affinity for CB2R, with K_i values spanning three orders of magnitude (0.18 to 187 nM), and, with the only exception of compounds **56**, **59** and **62**, fifteen of them proved to be potent CB2R ligands with K_i values in the range 0.18 – 27.1 nM. Only compounds **49**, **51**, **52**, **53** and **55** showed also significant affinity for CB1R, with K_i values in the medium nanomolar range (33.5 – 86.9 nM). Nevertheless, only compound **52** exhibited low receptor selectivity, while the other four pyrazolopyridine derivatives **49**, **51**, **53** and **55** had selectivity index values between 28 and 167. A higher SI (37 – 253) was found for compounds with low CB1R affinity, except for compound **62** (SI = 5), which resulted the poorest cannabinoid receptor ligand of the series.

We selected the most potent and selective compounds (i.e. **45**, **47**, **48**, **50**, **51**, **53**, **54**, **58**, **60**, **61**) for additional in vitro pharmacological evaluation to assess their ability to functionally activate the CB2R. We performed the cAMP Hunter™ assay, to measure intracellular cAMP levels, with enzyme fragment complementation technology in NKH-477-stimulated CHO cells optimized to overexpress CB2R. As shown in Figure 1, compounds (**51**, **53**, **54**, **55**, and **60**) activated the receptor with typical agonist behavior by reducing cAMP levels induced by the NKH-477 (a water-soluble analog of forskolin) as expected for a G_i protein-coupled receptor agonist.

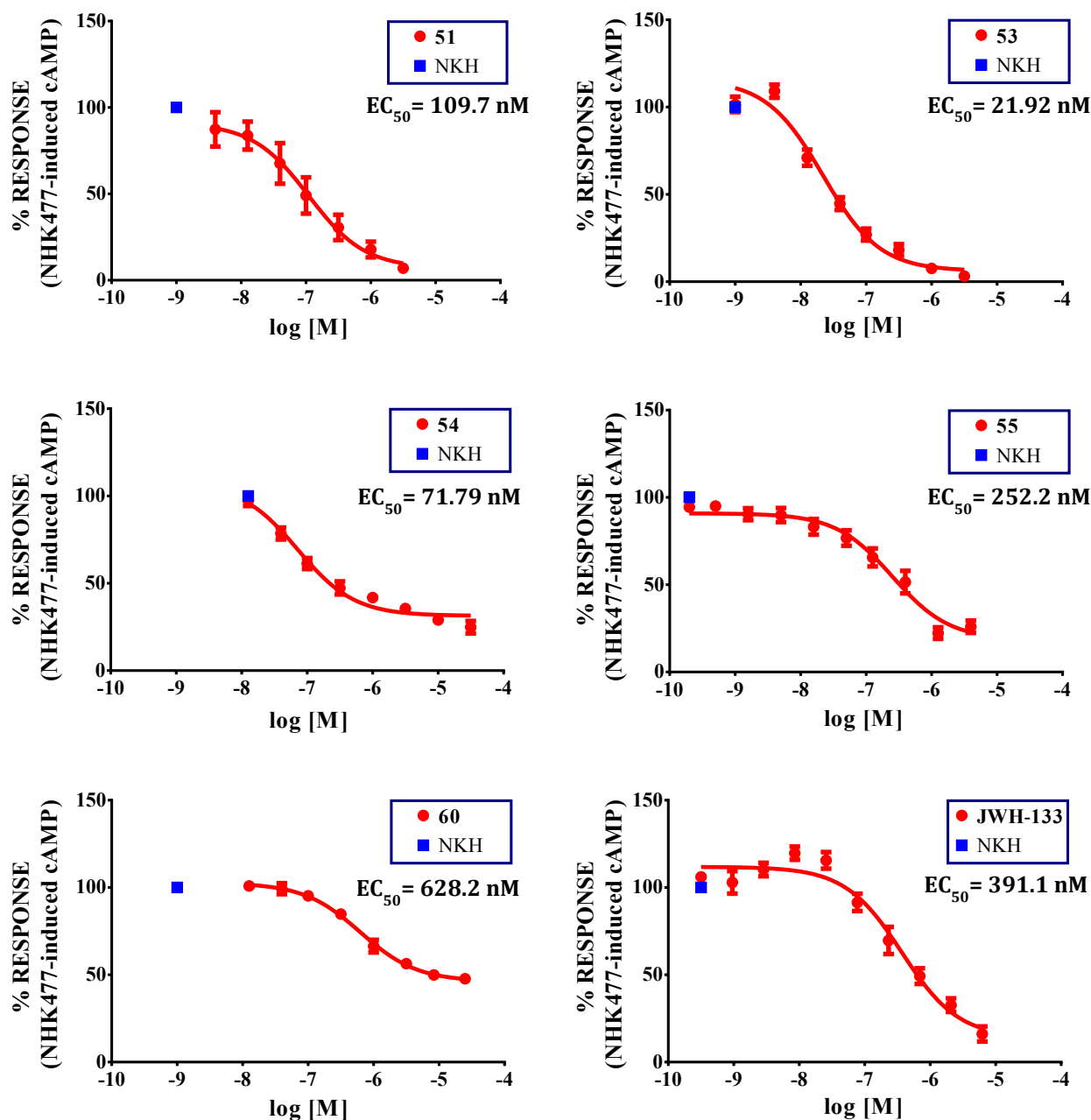


Figure 1. Concentration-response curves of compounds in cAMP Hunter™ assay enzyme fragment complementation chemiluminescent detection kit. The curves show the effect of increasing concentrations of compounds on NKH-477-induced cAMP levels in stable CHO cells expressing the human CB2R. Effect of JWH-133 is reported as reference compound. Data are reported as mean \pm SEM of three independent experiments conducted in triplicate and were normalized considering the NKH-477 stimulus alone as 100% of the response as indicated in the experimental session. EC_{50} was

determined by Graph Pad Prism 5 as the concentration that provokes the response halfway between the baseline (Bottom) and maximum response (Top) of the fitted dose-response.

Conversely, N2 substitution on the pyrazolopyridine moiety (compounds **45**, **47**, **48**, **49**, **50**, **58**, **61**) promoted a switch to an antagonist (**48** and **58**) or inverse agonist (compounds **45**, **47**, **49**, **50**, **61**) behavior, the latter being suggested by the ability of these compounds to increase the levels of NKH-477 induced cAMP (not shown). To further confirm this hypothesis, compounds **45**, **47**, **48**, **50**, **58** and **61** were also tested in the presence of an EC₈₀ concentration of a CB2-ligand (4 μ M of JWH-133). The compounds were able to antagonize JWH-133-induced inhibition of NKH-477 induced cAMP formation and, with the exception of **48** and **58**, up to levels higher than those induced by NKH-477 alone (considered as 100% response), thus confirming their predicted behavior (Figure 2).

Structure-Activity Relationship. Based on our previous findings,^{21,25} in all compounds the adamantane moiety was retained, with either no modification or the one modification represented by the insertion of a hydroxy group at the 3'-position. This change resulted in some decrease of affinity at CB2R, as evident by comparing couples of compounds (**45/46**, **47/48**, **51/52**, and **58/59**) differing from each other only in this respect.

A major impact on receptor affinity was exerted by the alkyl chain at N4. The stepwise lengthening of this chain from 3 (**56**) to 4 (**57**) or 5 (**58**) carbon atoms caused a progressive improvement in CB2R binding, but the chain was not elongated further to avoid an excessive increase of lipophilicity. Conversely, we took into consideration the frequently used strategy of incorporating fluorine into drug molecules, aimed at improving potency and optimizing physicochemical and ADME properties.³¹ This approach has ensured beneficial effects during lead optimization programs, when attention was paid to the corresponding changes in a number of parameters of the drug candidate.³² Accordingly, we opted for the replacement with fluorine of a hydrogen atom of the terminal methyl group in the 4-carbon atom chain, by evaluating at the same time the benefits of this modification in terms of binding affinity and lipophilic ligand efficiency (*vide infra*).

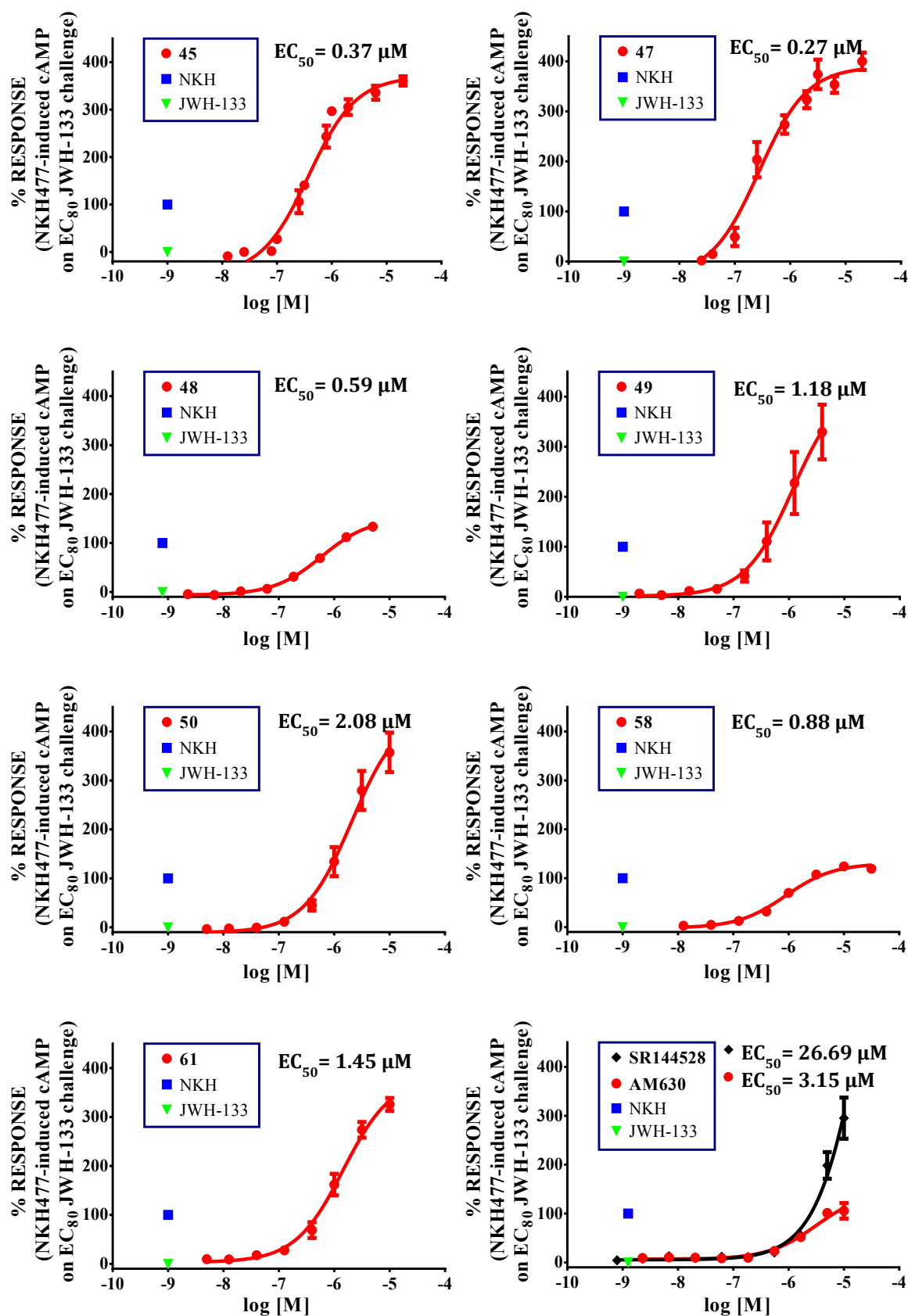


Figure 2. Concentration-response curves of compounds in cAMP Hunter™ assay. Curves show the effect of increasing concentrations of compounds on NKH-477-induced cAMP levels and in presence

of an EC₈₀ CB2-ligand challenge (4 μ M of JWH-133), in stable CHO cells expressing the human CB2. Data are reported as mean \pm SEM of three independent experiments conducted in triplicate, and were normalized to the maximal and minimal response as indicated in the experimental session. EC₅₀ was determined by Graph Pad Prism 5 as the concentration that provokes the response halfway between the baseline (Bottom) and maximum response (Top) of the fitted dose-response.

Comparison between **45/47**, **46/48**, **51/53**, and **52/54** clearly shows that no substantial change in CB2R affinity occurred as a consequence of hydrogen/fluorine exchange; in all cases, a very slight increase in affinity could be measured instead, associated with an improvement in receptor selectivity. On the other hand, the insertion at the end of the alkyl chain of a hydroxyl (**61**) or an acetoxyl (**50**) group led to a 6/7-fold decrease in binding affinity at CB2R with concurrent loss of affinity for the other receptor subtype.

A longer chain with an H-bond donor/acceptor hydroxyl was also substituted for the N2-methyl group to get more information on the structure-activity relationship (SAR). Compounds **56-59** exhibited significantly lower CB2R affinity than their methylated counterparts; similar result was also yielded by compound **60** compared to its N1-methyl analog **51**.

The structure-function relationship appears to be very well defined and strictly dependent on N1 or N2 substitution. N1-Methyl substituted derivatives **51**, **53**, **54**, **55**, **60** show the ability to activate the CB2R, while the corresponding compounds with the methyl substituent at N2 position behave as inverse agonists (**45**, **47**, **49**, **50**, **61**) or neutral antagonists (**48** and **58**) at the same receptor. Modification of other structural features, such as the N4 chain or adamantane moiety, were irrelevant in this regard.

Estimated Druglike Properties.

The molecular properties of tested compounds **45-62** were estimated using the free web tool SwissADME [<http://www.swissadme.ch>] and compared to those of compounds **1** and **2** (Table 1S, Supporting Information), that previously proved to be very potent and selective CB2R ligands, but

did not exhibit completely satisfactory physicochemical characteristics. Overall, the new pyrazolo[4,3-*b*]pyridine derivatives were in line with the general druglikeness requirements, possessing better virtual profiles than compounds **1** and **2** according to the Lipinski's "rule-of-five" (Ro5),³³ Veber's parameters,³⁴ and lipophilic ligand efficiency (LLE)³⁵. In particular, the calculated Log *P* (CLogP) and TPSA values for many of the compounds **45-62** fell within the optimal range for oral bioavailability and blood–brain barrier (BBB) permeability (CLogP = 2–4, TPSA = 50–90 Å²),³⁶ while the higher polarity (TPSA = 109–129 Å²) estimated for some of them prompt to presume that these compounds might be predominantly peripheral CB2R binders, as their ability to penetrate the CNS may be expected to be lower.³⁷ Sixteen of the eighteen compounds were characterized by a multi-parameter score LLE within the optimal range for suitable drug candidates (5 < LLE < 7), since the reduction in overall lipophilicity, as predicted by CLogP values, did not affect the CB2R affinity values (p*K*_{CB2}).

In Vitro Physicochemical Characterization. The aqueous solubility of compounds **45-62** was then assessed measuring their kinetic solubility starting from DMSO stock solutions.²⁵ This approach was preferred to measurements of equilibrium solubility from powder, because these are significantly affected by the nature of the solid state (amorphous, crystalline, presence of different polymorphs, solvates), which, generally, is not thoroughly investigated at these stages of drug development. In Table 2 the values of kinetic solubility, at pH 1.0 and 7.4, expressed as µg/mL, are reported.

Table 2. Experimental and Calculated Solubility of Compounds 45-62 in Comparison with Compounds 1 and 2

Compd	Kinetic	Kinetic	Kinetic	Calculated	Calculated
	Solubility	Solubility	Solubility	Solubility	Solubility
	pH 1.0	pH 7.4	pH 7.4	ACD/Labs ^b	ALOGPS ^c
	(µg/mL) ^a	(µg/mL) ^a	Log <i>S</i>	Log <i>S</i>	Log <i>S</i>

45	0.23 ± 0.03	1.9 ± 0.3	-5.32	-4.38	-3.64
46	15 ± 2	20.9 ± 0.8	-4.32	-3.36	-2.76
47	0.6 ± 0.1	0.8 ± 0.1	-5.73	-4.51	-3.72
48	39.9 ± 0.2	37.6 ± 1.3	-4.06	-3.49	-2.72
49	2.9 ± 0.2	1.9 ± 0.2	-5.35	-4.65	-4.01
50	^d	1.3 ± 0.2	-5.54	-4.26	-3.81
51	0.13 ± 0.01	0.49 ± 0.06	-5.96	-4.32	-3.67
52	2.1 ± 0.6	4.6 ± 0.3	-4.95	-3.32	-2.79
53	0.7 ± 0.2	1.5 ± 0.4	-5.52	-4.46	-3.77
54	9.1 ± 0.1	15.1 ± 0.2	-4.45	-3.45	-2.78
55	0.4 ± 0.1	1.08 ± 0.04	-5.58	-4.65	-4.02
56	3.4 ± 0.6	3.9 ± 0.1	-5.03	-3.95	-2.99
57	1.6 ± 0.2	2.1 ± 0.4	-5.30	-4.22	-3.32
58	0.38 ± 0.05	0.70 ± 0.02	-5.80	-4.49	-3.66
59	9.70 ± 0.02	15 ± 1	-4.49	-3.46	-2.89
60	0.11 ± 0.03	0.24 ± 0.04	-6.26	-4.20	-3.29
61	2.53 ± 0.06	3.2 ± 0.1	-5.11	-3.61	-3.06
62	^d	1.1 ± 0.1	-5.61	-4.28	-3.77
1^e	0.21 ± 0.02	1.0 ± 0.1	-5.64	-6.04	-6.15
2^e	0.23 ± 0.06	1.4 ± 0.1	-5.47	-4.47	-4.99

^aReported are mean values together with Standard Deviation (n = 4). ^bACD calculated solubility values (ACD/Labs I-Lab 2.0: <http://www.ilab.acdlabs.com>). ^cALOGPS 2.1 calculated solubility values (<http://www.vcclab.org>). Reported are the mean solubility values of the neutral species calculated taking into account the different tautomeric forms reported in Figure 2S (Supporting

Information). ^d Not stable in the test time period (> 25% hydrolysis of the side chain ester group in 4 h). ^e See also reference 25.

The corresponding Log *S* values, in Log (mol/L) scale are compared to calculated Log *S* by ACD/Labs and ALOGPS software. In general, experimental Log *S* at acidic pH (pH 1.0) ranged between –4.03 of the most soluble **48** and –6.59 of the least soluble **60** and between –4.06 (**48**) and –6.26 (**60**) at physiological pH, spanning over two orders of magnitude. The values of log *S* calculated by the two software, ACD/Labs and ALOGPS respectively, were mutually correlated (Log *S*_{ACD} = 0.97(±0.08) Log *S*_{ALOGPS} –0.77(±0.27); *n* = 18; *r*² = 0.905; *s* = 0.15; *F* = 152), but tended to overestimate solubility in comparison with experimental results. Correlation between experimental and calculated values was significantly lower, with ACD/Labs (Log *S*_{exp} = 1.01(±0.19) Log *S*_{ACD} –1.15(±0.77); *n* = 18; *r*² = 0.641; *s* = 0.37; *F* = 28.5) performing better than ALOGPS (Log *S*_{exp} = 0.98(±0.21) Log *S*_{ALOGPS} –1.93(±0.71); *n* = 18; *r*² = 0.580; *s* = 0.40; *F* = 22.1).

Considering experimental results, in the subset of N2-methyl derivatives **45-50** and **61**, hydroxylation of the adamantyl group (**46**) led to a 1-log unit increase in solubility at both pHs, if compared to the parent compound **45**. Fluorination of the butyl side chain at N4 (**47**) increased the solubility at acidic pH (3 times *vs.* **45**), but led to a slight decrease at physiological pH. The combination of both hydroxylation and fluorination gave the best result, with a solubility for compound **48** 170 times (pH 1.0) and 20 times (pH 7.4) higher than that of **45**. Within the subset of N2-methyl substituted derivatives, shifting from *n*-butyl to *n*-pentyl side chain at N4 (**49**) did not significantly affect kinetic solubility, especially at physiological pH, whereas hydroxylation of the side chain (**61**) led to an increase in the solubility at both pHs, even if the magnitude of the effect was not comparable to that obtained with 3'-hydroxylation at the adamantyl ring. Acetylation of the hydroxyl group in the side chain (**50**) did not significantly affect solubility at pH 7.4 and led to a stability issue owing to hydrolysis of this ester group at acidic pH. N1-Methyl derivatives **51-55** were in general less soluble at both pHs than the corresponding N2-methyl ones. For instance, parent compound **51** was twice

less soluble at pH 1.0 and four times less soluble at pH 7.4 than corresponding **45**. Nevertheless, 3'-hydroxylation at the adamantyl group (**52**), fluorination on the *n*-butyl side chain at N4 (**53**) and the combination of both substitutions (**54**) paralleled the effects on kinetic solubility observed for the **46-48** subset. Compound **54** was the most soluble of N1-methyl derivatives with a Log *S* at physiological pH around -4.45.

Finally, the combined effect on kinetic solubility of introducing a hydroxyethyl side chain at N1 (**60**) or N2 (**56-59**) of the 5-oxopyrazolo[4,3-*b*]pyridine nucleus and of elongating the side chain at N4 was explored, looking for the right combination of both solubility and activity. As previously observed, the N1-substituted derivative (**60**) was much less soluble than the corresponding N2-substituted one (**57**) and also the pharmacological activity and selectivity for CB2R favored the latter. Elongation of the alkyl side chain at N4 led to a 1-log unit progressive decrease in kinetic solubility at both pHs (**56-58**). Compound **57** combined good selectivity for CB2R (SI > 54) with a Log *S* = -5.30. The ionization constants (p*K*_a) and experimental lipophilicity (log *P*_{oct}) of compounds **45**, **46**, **48**, **51**, and **52** were also measured, by means of a UV-metric and potentiometric approach (see Experimental Section and Table 3).³⁸

Table 3. Ionization Constants (p*K*_a) and Lipophilicity (Log *P*_{oct}) of Compounds 45, 46, 48, 51, and 52

Compd	p <i>K</i> _a ^{a,b}	Log <i>P</i> _{oct} ^{b,c}
45	8.6 ± 0.1	5.3 ± 0.1
46	7.9 ± 0.1	4.08 ± 0.05
48	7.97 ± 0.07	3.15 ± 0.01
51	8 ± 0.1	5.3 ± 0.1
52	7.56 ± 0.05	4.85 ± 0.01

^a Aqueous p*K*_a values extrapolated from MeOH/0.15 M ionic strength adjusted water solutions (see

Experimental Section for details). ^bReported are mean values together with their Standard Deviations (n=3). ^c Measured by the potentiometric pH-metric approach.³⁸

For all compounds, aqueous pK_a values were extrapolated starting from solutions at different percentages of co-solvent (MeOH). In all the cases, the slope of the extrapolation curve was typical of acidic compounds. Measured pK_a values ranged from 7.56 (**52**) to 8.56 (**45**). In both subsets of N2-methyl (**45**, **46**) and N1-methyl (**51**, **52**) substituted derivatives, the introduction of the hydroxyl group at 3' on the adamantyl ring led to a significant decrease in pK_a value, while no effect was seen for fluorination (**48**). The partition coefficients (log *P*_{oct}) were determined evaluating the shifts produced in the titration curves by different ratios of partition solvent (*n*-octanol) and 0.15 M ionic strength adjusted water. Remarkably, in the N2-methyl derivatives (**45**, **46**, **48**) a 2-log unit decrease of lipophilicity was observed when 3'-hydroxylation on adamantane or N4-side chain fluorination took place. Experimental log *P* values differed from calculated ones by a Δ(log *P*_{oct} – CLogP) ranging between 1.2 and 1.6, except for compound **52**, which rather surprisingly showed an experimental log *P* value significantly higher than the corresponding N2-substituted isomer **46**. However, the experimental values paralleled the calculated ones and compounds **45**, **46**, **48**, **51**, and **52** ranked in the same order based on both theoretical and experimental lipophilicity. Therefore, the calculation of druglikeness was useful to predict how structural modifications of compounds would affect their main physicochemical properties.

In Vitro Cytotoxicity. In vitro cytotoxicity and cytocompatibility testing provides a crucial means of ranking compounds for consideration in drug discovery. Although all the molecules of the series were tested for cytotoxicity, only compounds which showed low cytotoxicity were reported.

To check the potentiality of these compounds, in vitro cell toxicity up to 24 hours towards either NIH3T3 fibroblasts or Normal Human Articular Chondrocytes (NHAC-kn) was assessed as a function of concentration, and results (IC₅₀ values) are reported in Table 4.

Table 4. Cytotoxicity Values of Selected Compounds 45-48, 50-54, 57-61 towards NIH3T3 Fibroblasts and Normal Human Articular Chondrocytes (NHAC-kn)^a

Compd	NIH3T3 (IC ₅₀ , μM)	NHAC-kn (IC ₅₀ , μM)
45	12.5	7.5
46	7.5	2.5
47	12.5	7.5
48	25	12.5
50	25	7.5
51	25	12.5
52	25	7.5
53	12.5	12.5
54	25	7.5
57	12.5	2.5
58	7.5	2.5
59	7.5	2.5
60	12.5	2.5
61	25	12.5

^aCell viability measured by the Neutral Red Uptake (NRU) test. All compounds were tested at increasing concentrations ranging from 2.5 to 50 μM. The assay was carried out three times in three replicates for each tested concentration. The standard deviation is less than 5%.

All the test compounds showed good cell compatibility and demonstrated to inhibit cell viability at micromolar concentrations: from 7.5 to 25 μM for NIH3T3 fibroblasts and from 2.5 to 12.5 μM for NHAC-kn.

Three compounds in particular (**48**, **51** and **61**) showed low cytotoxicity (IC₅₀>10 μM) against both cell types. Based on its functionality at CB2R and drug-like properties, we selected **51** as the lead

compound, which was further investigated for its long lasting cytotoxicity and capability of blocking the in vitro dedifferentiation process of human chondrocytes. Cell viability of NHAC-kn exposed to 7.5 μ M, i.e. the highest not toxic concentration, up to 14 days was assessed by the Neutral Red Uptake assay. As shown in Table 5, no toxic effect towards chondrocyte viability was observed as cell density was not statistically different ($p < 0.05$) in comparison with vehicle at 1, 7, and 14 days, demonstrating that compound **51** does not interfere with NHAC-kn cell viability.

Table 5. Percentage of Viable NHAC-kn in Contact with Compound 51 (7.5 μ M) Evaluated by the Neutral Red Uptake Test as a Function of Incubation Time

	Percentage (\pm SD) of viable NHAC-kn as a function of incubation time		
	1 day	7 days	14 day
Negative control (Growth Medium)	47 \pm 6	73 \pm 8	100 \pm 11
Compound 51 (7.5 μM)	*51 \pm 8	*68 \pm 6	*94 \pm 7

Data are means \pm SD of three replicates for each tested concentration or incubation time. *Data are not statistically different in comparison to negative control, $p < 0.05$.

NHAC-kn in contact with 7.5 μ M compound **51** were analysed for their content of major cartilaginous extra-cellular matrix (ECM) components, i.e. sulphated GAG and total collagen (HYP), in order to assess the ability of the test compound to prevent chondrocytes dedifferentiation. In fact, human chondrocytes dedifferentiate rapidly during monolayer culture, acquiring a fibroblast-

1
2
3
4
5
6
7
8
9
10
11
12
13
14
15
16
17
18
19
20
21
22
23
24
25
26
27
28
29
30
31
32
33
34
35
36
37
38
39
40
41
42
43
44
45
46
47
48
49
50
51
52
53
54
55
56
57
58
59
60

like phenotype and decreasing the production of cartilaginous tissue. As reported in Table 6, compound **51** statistically increased sGAG levels compared to the negative control, i.e. growth medium not supplemented with growth factors able to decelerate the dedifferentiation process,³⁹ already after 7 days and its effect persisted after 14 days of incubation. The increase in sGAG levels is a significant result, as it shows that chondrocytes are not differentiated.

Hydroxyproline (HYP) is a non-proteinogenic amino acid formed by the post-translational hydroxylation of proline. HYP is a major component of collagen, where it serves to stabilize the helical structure. Because HYP is largely restricted to collagen, the measurements of HYP levels can be used as an indicator of collagen content.

The results obtained regarding HYP production by human chondrocytes in contact with negative control and 7.5 μ M compound **51**, are reported in Table 6.

Table 6. Extracellular Matrix Production in NHAC-kn Cultures in the Presence of Growth Medium (Negative Control) or Compound 51 (7.5 μ M) as a Function of Incubation Time.

Incubation time	Extracellular matrix production					
	sGAG (μ g \pm SD)		HYP (μ g \pm SD)		sGAG/HYP ratio	
	Negative control	Compound 51	Negative control	Compound 51	Negative control	Compound 51
1 day	9.3 \pm 0.2	8.9 \pm 0.4	9.9 \pm 0.3	10.1 \pm 0.2	0.9 \pm 0.1	0.9 \pm 0.2
7 days	11.2 \pm 0.4	*12.6 \pm 0.3	13.2 \pm 0.3	12.9 \pm 0.3	0.8 \pm 0.2	1 \pm 0.2
14 days	12.0 \pm 0.4	*14.2 \pm 0.3	14.2 \pm 0.4	13.9 \pm 0.3	0.9 \pm 0.2	1 \pm 0.2

Data are means \pm SD of three replicates for each incubation time.

*Data are significantly different in comparison to the negative control. $p<0.05$.

The data demonstrate that the amount of HYP increased by increasing the incubation time for both the negative control and test compound of the same extent. The increasing of both sGAG and HYP

levels, and the value of the sGAG/HYP ratio, calculated as an indicator for hyaline or fibrocartilage nature of the produced matrix (Table 6), demonstrated that negative control and compound **51** showed the same trend and that the sGAG/HYP ratio remained constant by increasing the incubation time. These results indicate that, although specific collagen was not measured, the produced extracellular matrix was hyaline. In addition, these results demonstrate the good ability of the compound **51** to stimulate the production of hyaline ECM and to prevent the in vitro dedifferentiation of primary human chondrocytes (HC) confirming its chondrogenic capacity.

Effect of CB2R Agonist Systemic Administration on Joint Hypersensitivity and Walking

Pattern in MIA-Treated Rats. To evaluate the analgesic properties of the lead compound in vivo, we induced osteoarthritis in rats by intraarticular injection of sodium monoiodoacetate (MIA), which prompts rapid pain-like responses in the ipsilateral limb and morphological changes of the articular cartilage. All changes of the micro-architecture of subchondral bone in terms of bone volume, trabecular thickness and trabecular number lead to bone disruption and cause knee joint hypersensitivity. Along with pain phenotype development, joint damage and subchondral bone disruption, MIA injection induces weight-bearing deficits that are measurable and quantifiable particularly 21 and 28 days post injection.^{40a} Moreover, osteoarthritis (OA) development is accompanied by dynamic changes of CB2 expression in dorsal root ganglion (DRG) and cartilage in MIA rats.^{41a,b} Therefore, 21 days after OA induction we assessed pain-related behaviors performing two different in vivo tests, test pressure applied measurement (PAM)^{40b,c} and the kinetic weight bearing (KWB) tests.^{40a} Two sensory systems were evaluated by joint hypersensitivity (PAM) and gait analysis (KWB) to well define the in vivo effect of compound **51** in OA-induced animals. In the PAM test, compound **51** triggered a statistically significant analgesic effect at the 1 mg/kg dose 60, 120 and 180 min after administration ($p < 0.05$ and $p < 0.01$, Figure 3).

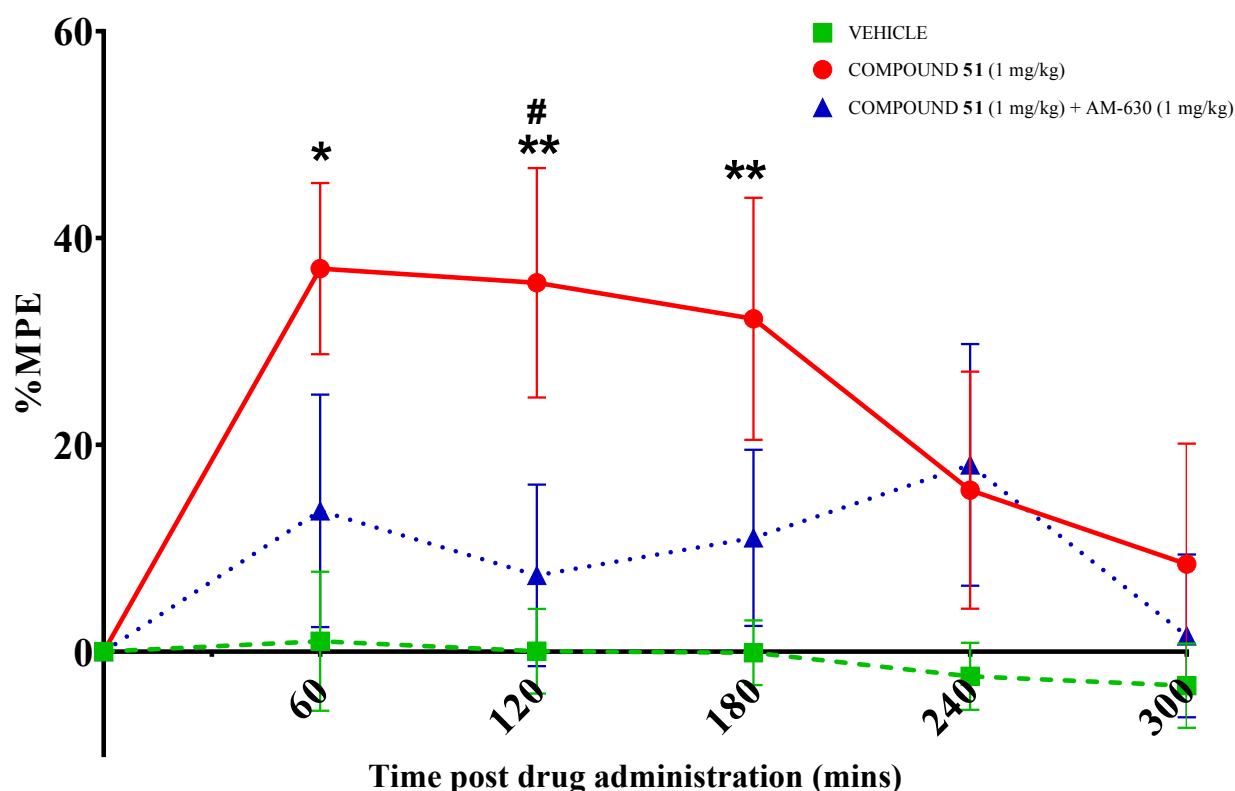


Figure 3. Time course and effect of acute, systemic treatment with compound **51** alone or in combination with the CB2 receptor antagonist AM-630 on hind limb joint hypersensitivity in osteoarthritic rats (PAM test). 21 or 28 days post injection with 1 mg of MIA, rats received compound **51** (1 mg/kg) intraperitoneally (i.p.), and the hind limb withdrawal threshold was assessed during a 300-min period. Compound **51** triggered a statistically significant analgesic effect (* $p < 0.05$ and ** $p < 0.01$) compared to the vehicle group at 60, 120, and 180 min post administration recordings. A systemic pre-administration of AM-630 (1 mg/kg, i.p.) reduced the analgesic effect of compound **51** with statistical significance (# $p < 0.05$) 120 min post injection. Data are presented as maximal possible effect (%MPE) \pm SEM. Male Wistar rats were used in the study and divided into four experimental groups with $n = 17$ for vehicle, $n = 10$ for compound **51**, $n = 10$ for AM-630 + compound **51**, $n = 6$ for AM-630. Statistical analysis was performed using analysis of variance (ANOVA) followed by Tukey post-hoc test. The values with $p < 0.05$ were considered significant. * denotes significant differences vs vehicle, # denotes significant differences vs compound **51** (1 mg/kg).

The effect of compound **51** (1 mg/kg, i.p.) was blocked by the CB2R antagonist AM630 (1 mg/kg, i.p.) 120 min. post administration (# $p < 0.05$), Figure 3). The injection of the vehicle solution had no *per se* analgesic effect. In the KWB test, a strong and significant difference between left and right paw peak force was detected in vehicle treated group ($p < 0.0001$, Figure 4).

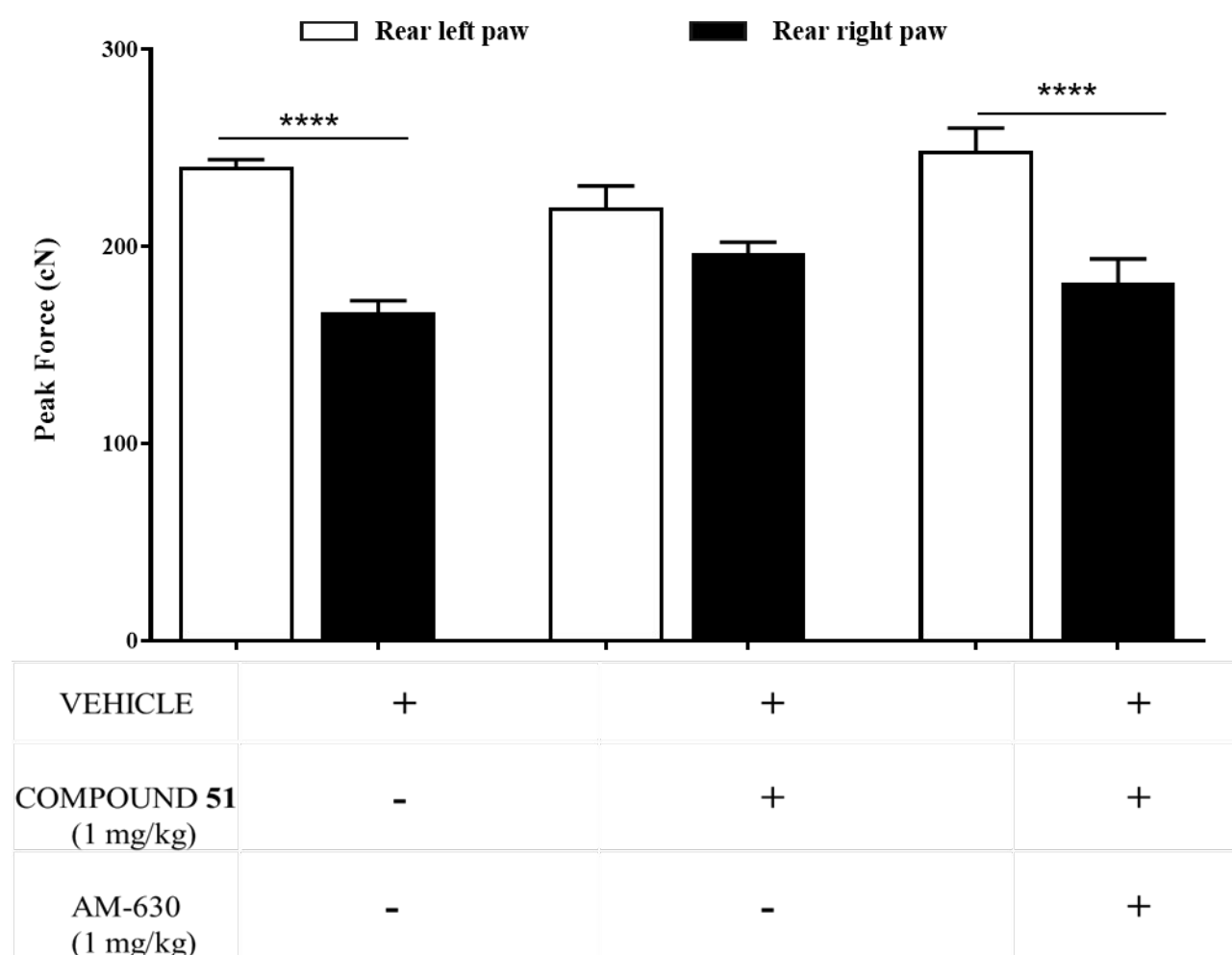
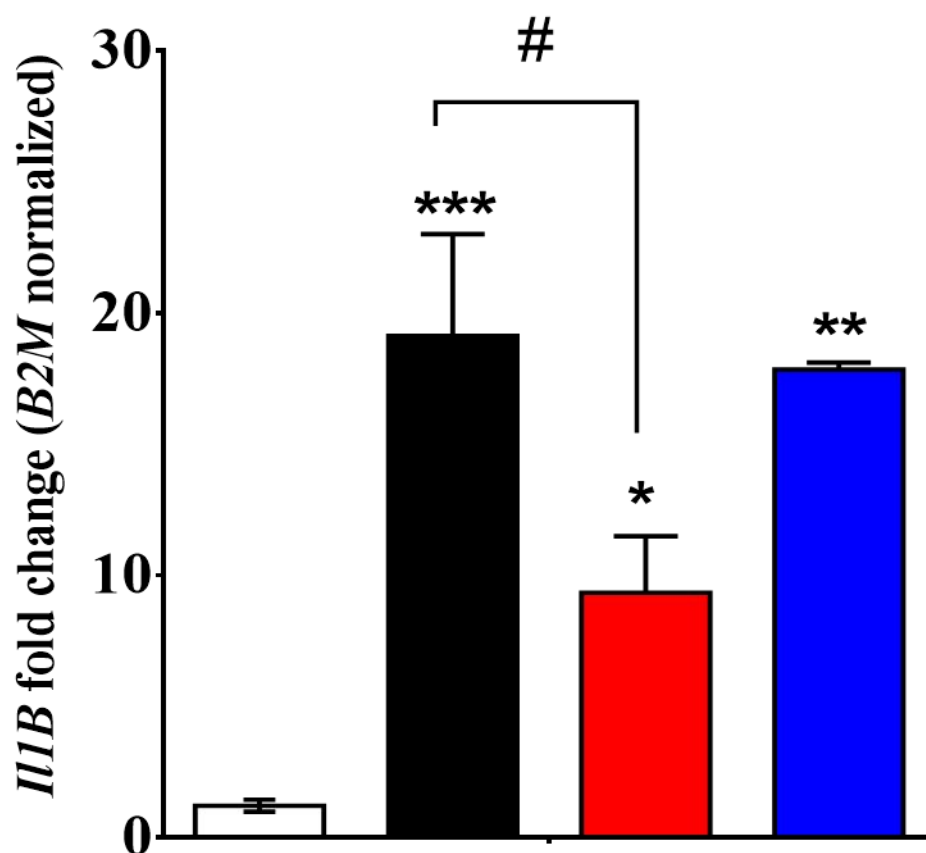


Figure 4. Effect of acute systemic administration of compound **51** alone or in combination with the CB2R antagonist AM-630 on kinetic weight bearing (KWB) test of MIA rats. On Days 21 and 28 post OA induction, MIA rats were monitored for differences in forces applied on the both rear paws during free walking movements and mechanical loading. The intraperitoneal (i.p.) administration of compound **51** (1 mg/kg) restored the differences in forces applied between rear left and rear right

(injured) paw 60 min post administration. A systemic pre-administration of AM-630 (1 mg/kg, i.p.) decreased the analgesic effect of compound **51** by reducing force applied on rear right (injured) paw, resulting in a disruption of rats walking pattern. Data are presented as mean \pm SEM. Male Wistar rats were used in the study and divided into four experimental groups with n = 22 for vehicle, n = 10 for compound **51**, n = 10 for AM-630 + compound **51**, n = 5 for AM-630. Statistical analysis was performed using analysis of variance (ANOVA) followed by Bonferroni post-hoc-test. The values with $p < 0.05$ were considered significant. * denotes significant differences rear left vs rear right paws in each group.

After administration of compound **51** (1 mg/kg) no statistical difference was observed between paws in respect to peak force ($p > 0.5$, Figure 4), indicating that the treatment restored disturbances in walking pattern of MIA rats. The effect was effectively blocked by AM630 ($p < 0.0001$), which *per se* was not able to restore walking pattern (not shown). These findings indicate that compound **51** holds both analgesic and anti-inflammatory properties, and that its actions are CB2-mediated.

Effect on Osteoarthritic Chondrocytes HC-OA Stimulated with TNF α . To better characterize the anti-inflammatory response of compound **51**, we stimulated human chondrocytes derived from human articular cartilage of donors with OA (HC-OA) with TNF α and we measured the mRNA expression of the *IL1B* gene encoding for IL-1 β , a pro-inflammatory cytokine that has been implicated in pain, inflammation and autoimmune conditions. Upon a 50 ng/mL stimulus with TNF α , we found a statistically significant increase of IL-1 β mRNA expression ($p < 0.001$) that was abolished ($p < 0.05$) in presence of 10 μ M of compound **51** (Figure 5). Co-incubation with the CB2 antagonist AM630 (1 μ M) did not affect *per se* the expression of pro-inflammatory cytokine IL-1 β (not shown), but was able to completely revert the anti-inflammatory effect of the full agonist compound **51** (Figure 5). Statistical analysis was performed using analysis of variance (ANOVA) followed by Dunnett post-hoc test, values with $p < 0.05$ were considered significant. * denotes significant differences vs vehicle group # denotes significant differences between vs TNF α group.



VEHICLE	+	+	+	+
TNFα (50 ng/ml)	-	+	+	+
COMPOUND 51 (10 μM)	-	-	+	+
AM-630 (1 μM)	-	-	-	+

Figure 5. Effect of compound **51** treatment alone or in combination with the CB2R antagonist AM-630 on IL-1 β expression in Human Osteoarthritic Chondrocytes (HC-OA) stimulated with TNF α . HC-OA derived from human articular cartilage of donors with OA were stimulated with TNF α (50 ng/mL) and the inflammatory response were measured by expression of the *Il1B* gene encoding for IL-1 β . Treatment with 10 μ M of compound **51** significantly reduced ($p < 0.001$) the mRNA levels of IL-1 β in the presence of TNF α . Co-treatment with AM-630 (1 μ M) abolished the anti-inflammatory effect of compound **51** restoring the high expression of *Il1B*. Data are presented as fold change (mean \pm SEM) normalized to expression of reference gene *B2m* and compared to the vehicle treated cells.

CONCLUSION

In this study, we have designed and synthesized a series of substituted pyrazolopyridinone amides starting from a quinolone series previously developed as CB2R ligands, but showing not completely satisfactory physicochemical characteristics. Structural optimization of quinolone derivatives was achieved by a scaffold hopping approach, involving the replacement of the benzene ring with the isosteric pyrazole, combined with the cautious introduction of the fluorine atom and/or hydroxy group aimed at the fine modulation of the overall properties of the compounds. Our efforts successfully provided 18 new cannabinoid ligands, most of which display CB2R affinity at low nanomolar or subnanomolar concentration, with 6 of them also showing good selectivity ($SI > 90$) over CB1R. In this series of compounds, both agonists and inverse agonists/neutral antagonists were identified, with functional activity strongly and exclusively depending on the substitution pattern of the pyrazole moiety. Most compounds in the series also display excellent physicochemical properties, mainly lipophilicity values that determine LLE scores ranging between 5.5-6.5. However, in general the experimental values of kinetic solubility at both acidic and neutral pH have not confirmed the calculated solubility, as most of the compounds still exhibit modest solubility in water despite a general reduction in lipophilicity. Nonetheless, 4 compounds (namely **46**, **48**, **54**, **59**) exhibit experimental solubility values approximately 75-200 times higher at acidic pH and 10-25 times higher at physiological pH compared to initial compounds **1** and **2**. This significant increase in solubility cannot be ascribed solely to the isosteric replacement of benzene with pyrazole, but rather to the concomitant contribution of other structural determinants, first of all the 3'-OH group on the adamantane moiety.

The results of in vivo evaluation in rats carrying induced osteoarthritis indicate that compound **51** exhibits both analgesic and anti-inflammatory activity and that this pharmacological profile is mediated by CB2R, thereby further confirming that the CB2R is a promising therapeutic target for diverse forms of tissue damage and inflammatory diseases, including osteoarthritis. Taken together,

these data suggest that the pyrazolopyrimidinone amides here described represent an excellent start towards further chemistry optimization of CB2R agonists and inverse agonists/antagonists as well as a remarkable tool for investigating the involvement of CB2R in diverse physiopathological conditions.

EXPERIMENTAL SECTION

General Information. Reagents were purchased from commercial suppliers and used without further purification. Anhydrous reactions were run under a positive pressure of dry N₂. Merck silica gel 60 was used for flash chromatography (23-400 mesh). ¹H NMR and ¹³C NMR were recorded at 400 and 100 MHz, respectively, on a Bruker Advance DPX400. Chemical shifts are reported relative to tetramethylsilane at 0.00 ppm. Mass spectral (MS) data were obtained using Agilent 1100 LC/MSD VL system (G1946C) with a 0.4 mL/min flow rate using a binary solvent system of 95:5 methanol/water. UV detection was monitored at 254 nm. Mass spectra were acquired either in positive or in negative mode scanning over the mass range of 105-1500. High resolution mass spectrometry (HRMS) measurements were performed using a Dionex Ultimate 3000 RS UHPLC system coupled to an Orbitrap™ Q-Exactive mass spectrometer (Thermo Scientific) operating in ESI positive ion mode full scan (m/z range 100-800 at resolution 70,000 FWHM at 200 m/z). Melting points were determined on a Gallenkamp apparatus and are uncorrected. Elemental analyses were performed on a Perkin-Elmer PE 2004 elemental analyzer and the data for C, H, and N are within 0.4% of the theoretical values. The chemical purity of most of the target compounds was determined using an Acquity Waters UPLC-MS system under the following conditions: Waters BEH C18 (2.1 mm x 50 mm, 1.7 μm) reversed phase column; method: gradient elution, solvent A (0.1% formic acid in water), solvent B (0.1% formic acid in acetonitrile) 90:10 to 0:100 over 2.9 min, flow rate of 0.5 mL/min, UV detector, 254 nm. The chemical purity of compounds **50**, **55**, and **61** was determined using an Agilent 1260 Infinity instrument constituted of a binary pump, an autosampler, an UV-DAD and an ESI-MS detector. The chromatographic separation was realized with a LiChrospher® 60 RP-

select B column (Merck) (4 x 150 mm, 5 μ m) injecting 20 μ L of the sample. Analysis was carried out with linear gradient elution of 0.1% (v/v) formic acid in water and acetonitrile/methanol mixture (50:50 v/v) at the flow rate of 0.6 mL/min. Gradient started from 100% of water reaching 2% in 12 min. UV detection was monitored at 254 nm. The purity of each compound was \geq 95% in either analysis. All tested compounds were also subjected to Pan-assay interference compounds (PAINS) filter,⁴² and none of them was filtered out as problematic structure.

Methyl 1-Methyl-4-nitro-1H-pyrazole-3-carboxylate (4) and Methyl 1-Methyl-4-nitro-1H-pyrazole-5-carboxylate (5). Methyl iodide (8.5 g, 0.06 mol) and potassium carbonate (8.29 g, 0.06 mol) were added to a solution of methyl 4-nitro-1H-pyrazole-3-carboxylate (5.13 g, 0.03 mol) in acetone (60 mL). The resulting mixture was warmed at 50 $^{\circ}$ C for 2 h, then concentrated under reduced pressure. The residue was treated with dichloromethane and water and the organic layer was washed with sodium thiosulfate solution and dried over anhydrous sodium sulfate. After evaporation of the solvent, the residue was purified by flash chromatography on silica gel. Elution with dichloromethane afforded the less polar isomer **5** (54% yield) as a light yellow solid; mp 45-47 $^{\circ}$ C (from dichloromethane) (lit. 38-41 $^{\circ}$ C).⁴³ 1 H NMR (400 MHz, CDCl_3): δ 8.00 (s, 1H), 3.99 (s, 6H). MS (ESI): m/z 186 $[\text{M}+\text{H}]^+$. Further elution of the column with dichloromethane/methanol (99:1 to 95:5) gave compound **4**; yield, 40%; white solid; mp 130-131 $^{\circ}$ C (from dichloromethane) (lit. 122-123 $^{\circ}$ C).⁴³ 1 H NMR (400 MHz, CDCl_3): δ 8.06 (s, 1H), 3.94 (s, 6H). MS (ESI): m/z 208 $[\text{M}+\text{Na}]^+$, 186 $[\text{M}+\text{H}]^+$.

Methyl 1-(2-Acetoxyethyl)-4-nitro-1H-pyrazole-3-carboxylate (6) and Methyl 1-(2-Acetoxyethyl)-4-nitro-1H-pyrazole-5-carboxylate (7). To a solution of methyl 4-nitro-1H-pyrazole-3-carboxylate (5.13 g, 0.03 mol) in acetone (60 mL) were successively added potassium carbonate (8.29 g, 0.06 mol), 2-bromoethyl acetate (10.0 g, 0.06 mol), and potassium iodide (8.3 g, 0.05 mol). The mixture was stirred at 50 $^{\circ}$ C for 24 h while further 2-bromoethyl acetate (2 x 0.03 mol) was added. After cooling, the mixture was concentrated and diluted with dichloromethane and water. The organic layer was washed with sodium thiosulfate solution, dried over anhydrous sodium

sulfate and evaporated to leave an oily residue which was purified by flash column chromatography. Elution with dichloromethane gave the first eluted isomer **7** in 30% yield; light yellow solid; mp 63-67 °C (from dichloromethane). ¹H NMR (400 MHz, CDCl₃): δ 8.00 (s, 1H), 4.50-4.48 (m, 2H), 4.37-4.35 (m, 2H), 3.95 (s, 3H), 1.95 (s, 3H). MS (ESI): *m/z* 258 [M+H]⁺. Further elution with dichloromethane/methanol (99:1 to 95:5) furnished compound **6**; yield, 60%; light yellow solid; mp 67-71 °C (from dichloromethane). ¹H NMR (400 MHz, CDCl₃): δ 7.97 (s, 1H), 4.48-4.46 (m, 2H), 4.35-4.33 (m, 2H), 3.93 (s, 3H), 1.92 (s, 3H). MS (ESI): *m/z* 258 [M+H]⁺.

Methyl 4-Amino-1-methyl-1H-pyrazole-3-carboxylate (8). To a solution of **4** (2 g, 10.8 mmol) in ethanol (200 mL), kept under stirring at 60 °C, iron powder (2.42 g, 43.8 mmol), anhydrous calcium chloride (1.19 g, 10.8 mmol), and water (50 mL) were added and the mixture was maintained at 60 °C for 3 h. After cooling to rt, the suspension was filtered through celite, concentrated to approximately 50 mL, and brought to pH 9 with 5% sodium carbonate solution. The white precipitate which formed was filtered out and the aqueous solution was extracted with ethyl acetate. The organic phase was washed with water, dried over sodium sulfate, and evaporated to dryness to leave compound **8** (78% yield) as a pale pink solid which was used in the next reaction with no need of purification. Mp 114-116 °C (from ethyl acetate) (lit. 97-102 °C).⁴³ ¹H NMR (400 MHz, CDCl₃): δ 6.80 (s, 1H), 3.95 (br s, 2H), 3.75 (s, 3H), 3.69 (s, 3H). MS (ESI): *m/z* 178 [M+Na]⁺.

Methyl 4-Amino-1-methyl-1H-pyrazole-5-carboxylate (9). Prepared from **5** according to the procedure described for the preparation of **8**. Yield, 91%; orange solid; mp 72-75 °C (from ethyl acetate) (lit. 65-68 °C).⁴³ ¹H NMR (400 MHz, CDCl₃): δ 6.94 (s, 1H), 4.63 (br s, 1H), 3.86 (s, 3H), 3.77 (s, 3H). MS (ESI): *m/z* 156 [M+H]⁺, 178 [M+Na]⁺.

Methyl 1-(2-Acetoxyethyl)-4-amino-1H-pyrazole-3-carboxylate (10). Prepared from **6** according to the procedure described for the preparation of **8**. Yield, 91%; reddish oil. ¹H NMR (400 MHz, CDCl₃): δ 6.93 (s, 1H), 4.30-4.27 (m, 2H), 4.20-4.71 (m, 2H), 3.79-3.77 (m, 3H), 1.92 (s, 3H). MS (ESI): *m/z* 228 [M+H]⁺, 250 [M+Na]⁺.

Methyl 1-(2-Acetoxyethyl)-4-amino-1H-pyrazole-5-carboxylate (11). Prepared from **7** according to the procedure described for the preparation of **8**. Yield, 73%; dark red solid; mp 69-73 °C (from ethyl acetate). ¹H NMR (400 MHz, CDCl₃): δ 7.02-7.01 (m, 1H), 4.56-4.53 (m, 2H), 4.28-4.24 (m, 2H), 3.96 (br s, 2H), 3.80-3.79 (m, 3H), 1.89-1.88 (m, 3H). MS (ESI) *m/z* 228 [M+H]⁺, 250 [M+Na]⁺.

Methyl 4-(1-Butylamino)-1-methyl-1H-pyrazole-3-carboxylate (12). 1-Iodobutane (416 mg, 2.26 mmol) was added to a solution of **8** (350 mg, 2.26 mmol) in dry DMF (3 mL) under a nitrogen atmosphere. The solution was gradually warmed to 50 °C and maintained at this temperature for 7 h. After cooling to rt, the solution was diluted with water (20 mL) and extracted with ethyl acetate. The organic layer was washed with 5% lithium chloride solution (4 x), water (2x), then brine, and was dried over anhydrous sodium sulfate. Removal of solvent gave an oily residue, which was purified by flash column chromatography on silica gel (petroleum ether/ethyl acetate, 1:1, as eluent) to provide **12** as a reddish oil; yield, 34%. ¹H NMR (400 MHz, CDCl₃): δ 6.74 (s, 1H), 4.70 (br s, 1H), 3.82 (s, 3H), 3.79 (s, 3H), 2.91 (t, *J* = 7.0 Hz, 2H), 1.55-1.48 (m, 2H), 1.38-1.28 (m, 2H), 0.86 (t, *J* = 7.3 Hz, 3H). MS (ESI): *m/z* 234 [M+Na]⁺.

Methyl 4-[(4-Fluoro-1-butyl)amino]-1-methyl-1H-pyrazole-3-carboxylate (13). Prepared from **8** according to the procedure described for the preparation of **12** using 1-bromo-4-fluorobutane as alkylating agent. Eluent, dichloromethane/methanol (100:1); yield, 30%; yellow oil. ¹H NMR (400 MHz, CDCl₃): δ 6.75 (s, 1H), 4.73 (br s, 1H), 4.46-4.44 (m, 1H), 4.35-4.32 (m, 1H), 3.81 (s, 3H), 3.78 (s, 3H), 2.99-2.95 (m, 2H), 1.76-1.40 (m, 4H). MS (ESI): *m/z* 252 [M+Na]⁺.

Methyl 1-Methyl-4-(1-pentylamino)-1H-pyrazole-3-carboxylate (14). Prepared from **8** according to the procedure described for the preparation of **12** using 1-iodopentane as alkylating agent. Eluent, petroleum ether/ethyl acetate (1:1); yield, 51%; yellow oil. ¹H NMR 400 MHz, CDCl₃): δ 6.79 (s, 1H), 3.86 (s, 3H), 3.82 (s, 3H), 2.94 (t, *J* = 6.9 Hz, 2H), 1.59-1.55 (m, 2H), 1.31-1.30 (m, 4H), 0.88-0.86 (m, 3H). MS (ESI): *m/z* 226 [M+H]⁺.

Methyl 4-[(4-Acetoxy-1-butyl)amino]-1-methyl-1H-pyrazole-3-carboxylate (15). Prepared from **8** according to the procedure described for the preparation of **12** using 4-iodobutyl acetate as

alkylating agent. Eluent, ethyl acetate; yield, 47%; yellow oil. ^1H NMR 400 MHz, CDCl_3): δ 6.74 (s, 1H), δ 4.72 (br s, 1H), δ 4.00-3.91 (m, 2H), δ 3.80 (s, 3H), δ 3.77 (s, 3H), δ 2.94-2.93 (m, 2H), δ 1.94 (s, 3H), δ 1.63-1.50 (m, 4H). MS (ESI): m/z 270 $[\text{M}+\text{H}]^+$.

Methyl 4-(1-Butylamino)-1-methyl-1H-pyrazole-5-carboxylate (16). Prepared from **9** according to the procedure described for the preparation of **12**. Eluent, petroleum ether/ethyl acetate (1:1); yield, 44%; yellow oil. ^1H NMR (400 MHz, CDCl_3): δ 6.91 (s, 1H), 4.46 (br s, 1H), 3.89 (s, 3H), 3.75 (s, 3H), 2.98 (t, $J = 7.0$ Hz, 2H), 1.50-1.43 (m, 2H), 1.32-1.23 (m, 2H), 0.82 (t, $J = 7.4$ Hz, 3H). MS (ESI): m/z 212 $[\text{M}+\text{H}]^+$, 234 $[\text{M}+\text{Na}]^+$.

Methyl 4-[(4-Fluoro-1-butyl)amino]-1-methyl-1H-pyrazole-3-carboxylate (17). Prepared from **9** using 1-bromo-4-fluorobutane as alkylating agent according to the procedure described for the preparation of **12**, although with some minor modifications. Since the reaction did not go to completion, after 24 h the mixture was separated by flash chromatography on silica gel, eluting with petroleum ether/ethyl acetate (1:1), to get product **17** and starting compound **9**, which was subjected again to the alkylation procedure, followed by product separation and purification. The title compound **17** could be obtained in this way in an overall yield of 30% for two runs as a yellow oil. ^1H NMR (400 MHz, CDCl_3): δ 6.96 (s, 1H), 4.46-4.43 (m, 1H), 4.34-4.31 (m, 1H), 3.94 (s, 3H), 3.80 (s, 3H), 3.08 (t, $J = 6.5$ Hz, 2H), 1.76-1.62 (m, 4H). MS (ESI): m/z 230 $[\text{M}+\text{H}]^+$, 252 $[\text{M}+\text{Na}]^+$.

Methyl 1-Methyl-4-(1-pentylamino)-1H-pyrazole-5-carboxylate (18). Prepared from **9** according to the procedure described for the preparation of **12** using 1-iodopentane as alkylating agent. Eluent, petroleum ether/ethyl acetate (2:1); yield, 50%; yellow oil. ^1H NMR (400 MHz, CDCl_3): δ 7.01 (s, 1H), 4.00 (s, 3H), 3.86 (s, 3H), 3.07 (t, $J = 5.8$ Hz, 2H), 1.60-1.57 (m, 2H), 1.33-1.32 (m, 4H), 0.88 (t, $J = 4.5$ Hz, 3H). MS (ESI): m/z 226 $[\text{M}+\text{H}]^+$.

Methyl 1-(2-Acetoxyethyl)-4-(1-propylamino)-1H-pyrazole-3-carboxylate (19). Prepared from **10** according to the procedure described for the preparation of **12** using 1-iodopropane as alkylating agent. Eluent, petroleum ether/ethyl acetate (1:1); yield, 48%; white crystals; mp 42-45 °C (from diethyl ether/petroleum ether, 1:1). ^1H NMR (400 MHz, CDCl_3): δ 6.78 (s, 1H), 4.70 (br s, 1H), 4.31

(m, 2H), 4.22 (m, 2H), 3.80 (s, 3H), 2.87 (m, 2H), 1.94 (s, 3H), 1.57-1.50 (m, 2H), 0.89 (m, 3H). MS (ESI): m/z 270 $[M+H]^+$.

Methyl 1-(2-Acetoxyethyl)-4-(1-butylamino)-1H-pyrazole-3-carboxylate (20). Prepared from **10** according to the procedure described for the preparation of **12**. Eluent, petroleum ether/ethyl acetate (1:1); yield, 42%; yellow oil. ^1H NMR (400 MHz, CDCl_3): δ 6.78 (s, 1H), 4.70 (br s, 1H), 4.31 (t, J = 5.3 Hz, 2H), 4.21 (t, J = 5.2 Hz, 2H), 3.79 (s, 3H), 2.89 (t, J = 6.9 Hz, 2H), 1.94 (s, 3H), 1.53-1.46 (m, 2H), 1.35-1.26 (m, 2H), 0.83 (t, J = 7.3 Hz, 3H). MS (ESI): m/z 284 $[M+H]^+$, 306 $[M+Na]^+$.

Methyl 1-(2-Acetoxyethyl)-4-(1-pentylamino)-1H-pyrazole-3-carboxylate (21). Prepared from **10** according to the procedure described for the preparation of **12** using 1-iodopentane as alkylating agent. Eluent, petroleum ether/ethyl acetate (1:1); yield, 40%; yellow oil. ^1H NMR (400 MHz, CDCl_3): δ 6.77 (s, 1H), 4.64 (br s, 1H), 4.31 (t, J = 5.3 Hz, 2H), 4.21 (t, J = 5.2 Hz, 2H), 3.79 (s, 3H), 2.87 (t, J = 7.0 Hz, 2H), 1.93 (s, 3H), 1.52-1.49 (m, 2H), 1.25-1.23 (m, 4H), 0.91-0.78 (m, 3H). MS (ESI): m/z 298 $[M+H]^+$, 320 $[M+Na]^+$.

Methyl 1-(2-Acetoxyethyl)-4-(1-butylamino)-1H-pyrazole-5-carboxylate (22). Prepared from **11** according to the procedure described for the preparation of **12**. Eluent, petroleum ether/ethyl acetate (1:1); yield, 34%; yellow oil. ^1H NMR (400 MHz, CDCl_3): δ 7.01 (s, 1H), 4.73 (br s, 1H), 4.55 (t, J = 5.4 Hz, 2H), 4.27 (t, J = 5.4 Hz, 2H), 3.79 (s, 3H), 3.02 (t, J = 7.0 Hz, 2H), 1.90 (s, 3H), 1.54-1.46 (m, 2H), 1.36-1.27 (m, 2H), 0.85 (t, J = 7.3 Hz, 3H). MS (ESI): m/z 284 $[M+H]^+$, 306 $[M+Na]^+$.

General Procedure for the Preparation of Derivatives 23-33. A solution of methyl 3-chloro-3-oxopropionate (0.12 mL, 1.11 mmol) in dry dichloromethane (2-3 mL) was added dropwise to an ice-cooled solution of amines **12-22** (0.74 mmol) and triethylamine (0.15 mL, 1.11 mmol) in dry dichloromethane (10 mL). After stirring at rt for 2 h, the solution was washed with saturated solution of sodium hydrogen carbonate, then 2 N HCl and brine. The organic layer was dried over anhydrous sodium sulfate and evaporated to give an oily residue, which was purified by flash column chromatography on silica gel. Elution with ethyl acetate/petroleum ether (2:1) yielded the amide derivatives **22-33**.

3-[*N*-(1-Butyl)-*N*-[3-(methoxycarbonyl)-1-methyl-1*H*-pyrazol-4-yl]amino]-3-oxopropanoic Acid Methyl Ester (**23**). Prepared from **12**; yield, 75%; light yellow oil. ¹H NMR (400 MHz, CDCl₃): δ 7.37 (s, 1H), 3.91 (s, 3H), 3.82 (s, 3H), 3.58 (s, 3H), 3.22-3.15 (m, 3H), 1.39-1.32 (m, 2H), 1.26-1.17 (m, 2H), 0.80 (t, *J* = 7.3 Hz, 3H). MS (ESI): *m/z* 312 [M+H]⁺, 334 [M+Na]⁺.

3-[*N*-(4-Fluoro-1-butyl)-*N*-[3-(methoxycarbonyl)-1-methyl-1*H*-pyrazol-4-yl]amino]-3-oxopropanoic Acid Methyl Ester (**24**). Prepared from **13**; yield, 59%; light yellow oil. ¹H NMR (400 MHz, acetone-d₆): δ 7.82 (s, 1H), 4.41 (t, *J* = 6.0 Hz, 1H), 4.29 (t, *J* = 5.9 Hz, 1H), 3.91 (s, 3H), 3.74 (s, 3H), 3.60-3.55 (m, 1H), 3.50 (s, 3H), 3.31-3.21 (m, 1H), 3.12 (s, 2H), 1.68-1.43 (m, 4H). MS (ESI) *m/z* 330 [M+H]⁺, 352 [M+Na]⁺.

3-[*N*-[3-(Methoxycarbonyl)-1-methyl-1*H*-pyrazol-4-yl]-*N*-(1-pentyl)]amino]-3-oxopropanoic Acid Methyl Ester (**25**). Prepared from **14**; yield, 81%; light yellow oil. ¹H NMR (400 MHz, CDCl₃): δ 7.42 (s, 1H), 3.96 (s, 3H), 3.88 (m, 5H), 3.64 (s, 3H), 3.20 (s, 2H), 1.45-1.41 (m, 2H), 1.27-1.24 (m, 4H), 0.83 (t, *J* = 6.7 Hz, 3H). MS (ESI) *m/z* 326 [M+H]⁺, 348 [M+Na]⁺.

3-[*N*-(4-Acetoxy-1-butyl)-*N*-[3-(methoxycarbonyl)-1-methyl-1*H*-pyrazol-4-yl]amino]-3-oxopropanoic Acid Methyl Ester (**26**). Prepared from **15**; yield, 54%; light yellow oil. ¹H NMR (400 MHz, CDCl₃): δ 7.37 (s, 1H), 3.87-3.86 (m, 2H), 3.84 (s, 3H), 3.73 (s, 3H), 3.45 (s, 3H), 3.22 (br s, 1H), 3.06 (m, 2H), 1.84 (s, 3H), 1.47-1.45 (m, 2H), 1.38-1.34 (m, 2H). MS (ESI) 392 [M+Na]⁺.

3-[*N*-(1-Butyl)-*N*-[5-(methoxycarbonyl)-1-methyl-1*H*-pyrazol-4-yl]amino]-3-oxopropanoic Acid Methyl Ester (**27**). Prepared from **16**; yield, 80%; light yellow oil. ¹H NMR (400 MHz, CDCl₃): δ 7.33 (s, 1H), 4.11 (s, 3H), 3.92 (s, 3H), 3.59 (s, 3H), 3.25-3.12 (m, 3H), 1.42-1.34 (m, 2H), 1.26-1.18 (m, 2H), 0.82 (t, *J* = 7.2 Hz, 3H). MS (ESI) *m/z* 312 [M+H]⁺, 334 [M+Na]⁺.

3-[*N*-(4-Fluoro-1-butyl)-*N*-[5-(methoxycarbonyl)-1-methyl-1*H*-pyrazol-4-yl]amino]-3-oxopropanoic Acid Methyl Ester (**28**). Prepared from **17**; yield, 58%; light yellow oil. ¹H NMR (400 MHz, CDCl₃): δ 7.31 (s, 1H), 4.39 (t, *J* = 5.8 Hz, 1H), 4.27 (t, *J* = 5.6 Hz, 1H), 4.07 (s, 3H), 3.88 (br s, 1H), 3.79 (s, 3H), 3.55 (s, 3H), 3.21 (br s, 1H), 3.09 (s, 2H), 1.66-1.46 (m, 4H). MS (ESI) *m/z* 330 [M+H]⁺, 352 [M+Na]⁺.

3-[*N*-[5-(Methoxycarbonyl)-1-methyl-1*H*-pyrazol-4-yl]-*N*-(1-pentyl)-amino]-3-oxopropanoic Acid Methyl Ester (**29**). Prepared from **18**; yield, 73%; light yellow oil. ¹H-NMR (400 MHz, CDCl₃) δ 7.38 (s, 1H), 4.16 (s, 3H), 3.87 (s, 3H), 3.64 (s, 3H), 3.17 (s, 2H), 1.48-1.41 (m, 2H), 1.30-1.23 (m, 6H), 0.84 (t, *J* = 6.2 Hz, 3H). MS (ESI) *m/z*: 348 [M+Na]⁺.

3-[*N*-[1-(2-Acetoxyethyl)-3-(methoxycarbonyl)-1*H*-pyrazol-4-yl]-*N*-(1-propyl)-amino]-3-oxopropanoic Acid Methyl Ester (**30**). Prepared from **19**; yield, 70%; light yellow solid; mp 73-75 °C (from diethyl ether). ¹H-NMR (400 MHz, CDCl₃) δ 7.44 (s, 1H), 4.34 (s, 4H), 3.80 (s, 3H), 3.55 (s, 3H), 3.12 (s, 2H), 1.93 (s, 3H), 1.42-1.33 (m, 2H), 0.78 (t, *J* = 8 Hz, 3H). MS (ESI) *m/z* 370 [M+H]⁺, 392 [M+Na]⁺.

3-[*N*-[1-(2-Acetoxyethyl)-3-(methoxycarbonyl)-1*H*-pyrazol-4-yl]-*N*-(1-butyl)-amino]-3-oxopropanoic Acid Methyl Ester (**31**). Prepared from **20**; yield, 81%; light yellow oil. ¹H-NMR (400 MHz, CDCl₃) δ 7.44 (s, 1H), 4.39-4.35 (m, 4H), 3.91 (br s, 1H), 3.83 (s, 3H), 3.58 (s, 3H), 3.14 (s, 3H), 1.96 (s, 3H), 1.37-1.32 (m, 2H), 1.27-1.17 (m, 2H), 0.81 (t, *J* = 7.2 Hz, 3H). MS (ESI) *m/z* 406 [M+Na]⁺.

3-[*N*-[1-(2-Acetoxyethyl)-3-(methoxycarbonyl)-1*H*-pyrazol-4-yl]-*N*-(1-pentyl)-amino]-3-oxopropanoic Acid Methyl Ester (**32**). Prepared from **21**; yield, 69%; light yellow oil. ¹H-NMR (400 MHz, CDCl₃) δ 7.43 (s, 1H), 4.32-4.30 (m, 4H), 3.78-3.75 (m, 4H), 3.53-3.49 (m, 3H), 3.10-3.08 (m, 3H), 1.94-1.88 (m, 3H), 1.33-1.30 (m, 2H), 1.14-1.10 (m, 4H), 0.73-0.70 (m, 3H). MS (ESI) *m/z* 398 [M+H]⁺, 420 [M+Na]⁺.

3-[*N*-[1-(2-Acetoxyethyl)-5-(methoxycarbonyl)-1*H*-pyrazol-4-yl]-*N*-(1-butyl)-amino]-3-oxopropanoic Acid Methyl Ester (**33**). Prepared from **22**; yield, 75%; light yellow oil. ¹H-NMR (400 MHz, CDCl₃): δ 7.33 (s, 1H), 4.73-4.64 (m, 2H), 4.38-4.31 (m, 2H), 3.79 (s, 3H), 3.54 (s, 3H), 3.18-3.13 (m, 1H), 3.09 (s, 2H), 1.86 (s, 3H), 1.37-1.30 (m, 2H), 1.24-1.13 (m, 2H), 0.78 (t, *J* = 7.3 Hz, 3H). MS (ESI) *m/z* 384 [M+H]⁺, 406 [M+Na]⁺.

General Procedure for the Preparation of Amides 45-60. A solution of the appropriate precursor **23-33** (0.96 mmol) in anhydrous THF (35 mL) was added dropwise to a suspension of 60% sodium hydride (77 mg, 1.92 mmol) in the same solvent (20 mL) containing dry methanol (20 μ L, 0.48 mmol). The reaction mixture was stirred at 60 °C for 2 h, then evaporated to leave a solid residue which was taken up into 5% sodium carbonate solution. The aqueous solution was extracted with diethyl ether to remove some starting material, then brought to pH 1 by adding 6 N HCl and extracted with ethyl acetate (3 x 20 mL). The organic layer was dried over anhydrous sodium sulfate, filtered, and evaporated to give the Dieckmann condensation products **34-44** as a solid residue insoluble in most organic solvents, which was used in the next step without purification. A mixture of the appropriate ester **33-44** (0.96 mmol), 1-aminoadamantane or 3-aminoadamantan-1-ol (1.92 mmol) in THF (3 mL) and toluene (10 mL) was refluxed for 1-2 h, while adding dropwise further toluene and distilling out the azeotropic mixture methanol/toluene. After completion of the reaction, solvent was removed under reduced pressure and the solid residue was taken up into ethyl acetate. The organic solution was washed successively with 2 N HCl and brine, then dried over anhydrous sodium sulfate, filtered, and concentrated to yield a solid residue which was purified by flash column chromatography on silica gel (ethyl acetate as eluent unless otherwise stated) and/or recrystallization as specified below to provide compounds **45-60**.

N-(Adamantan-1-yl)-4-(1-butyl)-4,5-dihydro-7-hydroxy-2-methyl-5-oxo-2H-pyrazolo[4,3-*b*]pyridin-6-carboxamide (**45**). Obtained from **34** and 1-aminoadamantane after recrystallization from methanol; yield, 67%; light yellow needles; mp 101-105 °C. ¹H NMR (400 MHz, CDCl₃): δ 17.68 (s, 1H), 11.30 and 10.21 (s, 1H), 7.22 (s, 1H), 4.01 (s, 3H), 3.83-3.78 (m, 2H), 2.07-2.03 (m, 10H), 1.70-1.56 (m, 7H), 1.35-1.26 (m, 2H), 0.87 (t, *J* = 7.3 Hz, 3H). ¹³C NMR (100 MHz, CDCl₃): δ 171.3, 169.2, 162.6, 132.0, 128.8, 114.3, 96.7, 52.4, 50.7, 45.1, 41.5, 40.6, 36.4, 29.6, 29.4, 20.3, 13.8. HRMS (ESI) *m/z* calcd for C₂₂H₃₀N₄O₃ [M+H]⁺ 399.2391 found 399.2390.

4-(1-Butyl)-4,5-dihydro-7-hydroxy-*N*-(1-hydroxyadamantan-3-yl)-2-methyl-5-oxo-2H-pyrazolo[4,3-*b*]pyridin-6-carboxamide (**46**). Obtained from **34** and 3-aminoadamantan-1-ol after recrystallization

from ethyl acetate; yield, 45%; white needles; mp 216-218 °C. ¹H NMR (400 MHz, CDCl₃): δ 18.61 and 17.47 (s, 1H), 11.41 and 10.32 (s, 1H), 7.26 and 7.23 (s, 1H), 4.02 (s, 3H), 3.83-3.79 (m, 2H), 2.23 (s, 2H), 2.07 (s, 2H), 1.97-1.94 (m, 2H), 1.69-1.46 (m, 11H), 1.36-1.27 (m, 2H), 0.88 (t, *J* = 7.3 Hz, 3H). ¹³C NMR (100 MHz, CDCl₃): δ 171.4, 169.0, 162.5, 131.8, 128.9, 114.4, 96.8, 77.4, 77.1, 76.8, 69.1, 54.6, 49.0, 45.1, 44.1, 40.7, 40.2, 34.9, 30.6, 29.6, 20.3, 13.8. HRMS (ESI) *m/z* calcd for C₂₂H₃₀N₄O₄ [M+H]⁺ 415.2340 found 415.2342.

N-(Adamantan-1-yl)-4,5-dihydro-4-(4-fluoro-1-butyl)-7-hydroxy-2-methyl-5-oxo-2H-pyrazolo[4,3-*b*]pyridin-6-carboxamide (**47**). Obtained from **35** and 1-aminoadamantane; purified by chromatography and recrystallization from methanol; yield, 59%; white pasty solid; mp 191-192 °C. ¹H NMR (400 MHz, CDCl₃): δ 17.74 (s, 1H), 11.38 and 10.18 (s, 1H), 7.25 (s, 1H), 4.48 (t, *J* = 5.4 Hz, 1H), 4.36 (t, *J* = 5.7 Hz, 1H), 4.02 (s, 3H), 3.90-3.86 (m, 2H), 2.07-2.04 (m, 8 H), 1.82-1.64 (m, 11 H). ¹³C NMR (100 MHz, CDCl₃): δ 171.3, 169.4, 162.6, 132.0, 128.6, 114.3, 96.6, 84.5, 82.8, 52.4, 44.6, 41.5, 40.6, 36.4, 29.4, 27.7, 27.5, 23.7, 23.6. HRMS (ESI) *m/z* calcd for C₂₂H₂₉FN₄O₃ [M+H]⁺ 417.2296 found 417.2294.

4,5-Dihydro-4-(4-fluoro-1-butyl)-7-hydroxy-*N*-(1-hydroxyadamantan-3-yl)-2-methyl-5-oxo-2H-pyrazolo[4,3-*b*]pyridin-6-carboxamide (**48**). Obtained from **35** and 3-aminoadamantan-1-ol after recrystallization from ethyl acetate; yield, 66%; white solid; mp 209-211 °C. ¹H NMR (400 MHz, CDCl₃): δ 18.53 and 17.52 (s, 1H), 11.43 and 10.27 (s, 1H), 7.26 (s, 1H), 4.50-4.47 (m, 1H), 4.38-4.35 (m, 1H), 4.02 (s, 3H), 3.90-3.87 (m, 2H), 2.24 (s, 2H), 2.07 (s, 2H), 2.02-1.95 (m, 2H), 1.80-1.62 (m, 11H), 1.59-1.46 (m, 2H). ¹³C NMR (100 MHz, CDCl₃): δ 171.4, 169.2, 162.6, 131.8, 128.7, 114.4, 96.7, 84.5, 82.8, 69.1, 54.7, 49.01, 44.7, 44.1, 40.7, 40.2, 34.9, 30.6, 27.7, 27.5, 23.7. HRMS (ESI) *m/z* calcd for C₂₂H₂₉FN₄O₄ [M+H]⁺ 433.2246 found 433.2249.

N-(Adamantan-1-yl)-4,5-dihydro-7-hydroxy-2-methyl-5-oxo-4-(1-pentyl)-2H-pyrazolo[4,3-*b*]pyridin-6-carboxamide (**49**). Prepared from **36** and 1-aminoadamantane and recrystallized from diethyl ether/petroleum ether; yield, 63%; white needles; mp 151-153 °C. ¹H NMR (400 MHz, CDCl₃): δ 18.58 and 17.50 (s, 1H), 11.39 and 10.25 (s, 1H), 7.27 (s, 1H), 4.06 (s, 3H), 3.84 (t, *J* = 7.7

Hz, 2H), 2.12-1.98 (m, 9H), 1.68-1.64 (m, 8H), 1.33-1.30 (m, 4H), 0.87 (t, $J = 6.8$ Hz, 3H). ^{13}C NMR (100 MHz, CDCl_3): δ 171.3, 169.2, 162.7, 132.1, 129.0, 114.2, 96.8, 52.4, 45.3, 41.6, 40.7, 36.4, 29.5, 29.1, 27.3, 22.5, 14.0. HRMS (ESI) m/z calcd for $\text{C}_{23}\text{H}_{32}\text{N}_4\text{O}_3$ $[\text{M}+\text{H}]^+$ 413.2547 found 413.2544.

*4-(4-Acetoxy-1-butyl)-N-(adamantan-1-yl)-4,5-dihydro-7-hydroxy-2-methyl-5-oxo-2H-pyrazolo[4,3-*b*]pyridin-6-carboxamide (50)*. Obtained from **37** and 1-aminoadamantane and purified by trituration with diethyl ether; yield, 49%; cream-coloured solid; mp 209-210 °C. ^1H NMR (400 MHz, CDCl_3): δ 18.50 and 17.64 (s, 1H), 10.17 (br s, 1H), 7.26 (s, 1H), 4.06-4.04 (m, 2H), 4.03 (s, 3H), 3.88-3.84 (m, 2H), 2.08-2.05 (m, 8H), 1.98 (s, 3H), 1.73-1.54 (m, 11H). ^{13}C NMR (100 MHz, CDCl_3): δ 171.3, 171.1, 169.4, 162.7, 132.1, 128.7, 114.2, 103.9, 96.7, 63.7, 52.4, 44.7, 41.5, 40.6, 36.4, 36.2, 29.4, 26.1, 24.1, 20.9. HRMS (ESI) m/z calcd for $\text{C}_{24}\text{H}_{32}\text{N}_4\text{O}_5$ $[\text{M}+\text{H}]^+$ 457.2445 found 457.2442.

*N-(Adamantan-1-yl)-4-(1-butyl)-4,5-dihydro-7-hydroxy-1-methyl-5-oxo-2H-pyrazolo[4,3-*b*]pyridin-6-carboxamide (51)*. Prepared from **38** and 1-aminoadamantane; purified by flash chromatography and recrystallization from methanol; yield, 52%; light yellow solid; mp 131-134 °C. ^1H NMR (400 MHz, CDCl_3): δ 18.72 and 18.20 (s, 1H), 11.02 and 10.41 (s, 1H), 7.35 and 7.32 (s, 1H), 4.22 and 4.16 (s, 3H), 3.93-3.88 (m, 2H), 2.07-2.04 (m, 10H), 1.69-1.58 (m, 7H), 1.37-1.28 (m, 2H), 0.88 (t, $J = 7.3$ Hz, 3H). ^{13}C NMR (100 MHz, CDCl_3): δ 171.7, 171.6, 169.3, 166.1, 166.0, 162.1, 130.3, 123.1, 122.9, 121.9, 95.5, 92.5, 53.1, 52.6, 44.4, 44.3, 41.6, 41.4, 39.2, 38.9, 36.3, 36.2, 30.2, 30.1, 29.4, 20.2, 20.0, 13.8, 13.7. HRMS (ESI) m/z calcd for $\text{C}_{22}\text{H}_{30}\text{N}_4\text{O}_3$ $[\text{M}+\text{H}]^+$ 399.2391 found 399.2390.

*4-(1-Butyl)-4,5-dihydro-7-hydroxy-N-(1-hydroxyadamantan-3-yl)-1-methyl-5-oxo-2H-pyrazolo[4,3-*b*]pyridin-6-carboxamide (52)*. Obtained from **38** and 3-aminoadamantan-1-ol after purification by flash chromatography followed by trituration with petroleum ether/diethyl ether (2:1); yield, 35%; white solid; mp 95-96 °C. ^1H NMR (400 MHz, CDCl_3): δ 18.73 and 17.99 (s, 1H), 11.08 and 10.51 (s, 1H), 7.37 and 7.34 (s, 1H), 4.23 and 4.17 (s, 3H), 3.95-3.89 (m, 2H), 2.24 (s, 2H), 2.08 (s, 2H), 2.03-1.94 (m, 2H), 1.66-1.50 (m, 11H), 1.38-1.31 (m, 2H), 0.91-0.87 (m, 3H). ^{13}C NMR (100 MHz,

CDCl₃): δ 171.9, 171.7, 166.0, 165.7, 162.0, 130.4, 127.8, 126.7, 123.2, 122.9, 121.2, 95.6, 92.6, 69.1, 55.2, 54.8, 49.0, 48.9, 44.6, 44.4, 44.2, 44.0, 40.3, 40.2, 39.2, 39.0, 34.9, 34.8, 30.1, 30.1, 30.1, 20.2, 20.0, 13.8, 13.7. HRMS (ESI) m/z calcd for C₂₂H₃₀N₄O₄ [M+H]⁺ 415.2340 found 415.2338.

N-(Adamantan-1-yl)-4,5-dihydro-4-(4-fluoro-1-butyl)-7-hydroxy-1-methyl-5-oxo-2H-pyrazolo[4,3-*b*]pyridin-6-carboxamide (**53**). Prepared from **39** and 1-aminoadamantane; purified by flash chromatography followed by recrystallization from methanol; yield, 30%; yellow crystals; mp 148-149 °C. ¹H NMR (400 MHz, CDCl₃): δ 18.68 and 18.24 (s, 1H), 11.03 and 10.37 (s, 1H), 7.36 and 7.34 (s, 1H), 4.46 (t, J = 5.6 Hz, 1H), 4.35 (t, J = 5.7 Hz, 1H), 4.22 and 4.16 (s, 3H), 4.00-3.94 (m, 2H), 2.10-2.02 (m, 10H), 1.85-1.76 (m, 2H), 1.69-1.61 (m, 7H). ¹³C NMR (100 MHz, CDCl₃): δ 171.7, 171.6, 169.4, 166.3, 166.2, 162.2, 130.1, 123.0, 122.8, 121.5, 95.6, 84.4, 84.2, 82.7, 82.6, 53.2, 52.7, 44.0, 43.9, 41.6, 41.4, 39.3, 39.1, 39.0, 36.3, 36.3, 29.4, 27.8, 27.6, 27.4, 24.2, 24.1. HRMS (ESI) m/z calcd for C₂₂H₂₉FN₄O₃ [M+H]⁺ 417.2296 found 417.2297.

4,5-Dihydro-4-(4-fluoro-1-butyl)-7-hydroxy-*N*-(1-hydroxyadamantan-3-yl)-1-methyl-5-oxo-2H-pyrazolo[4,3-*b*]pyridin-6-carboxamide (**54**). Obtained from **39** with 3-aminoadamantan-1-ol; purified by flash chromatography followed by trituration with petroleum ether/diethyl ether (2:1); yield, 44%; white solid; mp 132-133 °C. ¹H NMR (400 MHz, methanol-*d*₄): δ 18.08 (s, 1H), 10.46 (s, 1H), 7.58 (s, 1H), 4.44 (t, J = 5.5 Hz, 1H), 4.33 (t, J = 5.8 Hz, 1H), 4.11 (s, 3H), 4.00-3.92 (m, 2H), 2.22 (s, 2H), 2.04 (s, 2H), 1.99 (s, 2H), 1.71-1.51 (m, 13H). ¹³C NMR (100 MHz, CDCl₃): δ 171.7, 165.9, 162.0, 130.2, 123.1, 122.9, 95.5, 84.4, 82.7, 82.6, 69.0, 55.3, 54.9, 54.8, 49.0, 48.9, 44.2, 44.1, 44.0, 10.3, 40.2, 10.1, 39.3, 39.0, 34.9, 34.8, 30.6, 27.8, 27.6, 27.5, 27.4, 24.2, 24.1, 24.0. HRMS (ESI) m/z calcd for C₂₂H₂₉FN₄O₄ [M+H]⁺ 433.2246 found 433.2247.

N-(Adamantan-1-yl)-4,5-dihydro-7-hydroxy-1-methyl-5-oxo-4-(1-pentyl)-2H-pyrazolo[4,3-*b*]pyridin-6-carboxamide (**55**). Prepared from **40** and 1-aminoadamantane; purified by recrystallization from petroleum ether/diethyl ether (1:1); yield, 76%; white needles; mp 126-128 °C. ¹H-NMR (400 MHz, CDCl₃) δ : 17.78 (s, 1H), 10.32 (s, 1H), 7.38 (s, 1H), 4.22 (s, 3H), 3.95 (t, J =

7.6 Hz, 2H), 2.15-2.11 (m, 5H), 1.70-1.74 (m, 6H), 1.52 (s, 10H), 0.89 (t, $J = 3.3$ Hz, 3H). ^{13}C -NMR (100 MHz, CDCl_3): δ 171.6, 166.0, 161.9, 130.0, 122.9, 98.9, 96.68, 52.7, 44.6, 41.4, 39.2, 36.3, 29.4, 29.1, 27.8, 22.5, 13.9. HRMS (ESI) m/z calcd for $\text{C}_{23}\text{H}_{32}\text{N}_4\text{O}_3$ $[\text{M}+\text{H}]^+$ 413.2547 found 413.2544.

N-(Adamantan-1-yl)-4,5-dihydro-7-hydroxy-2-(2-hydroxyethyl)-5-oxo-4-(1-propyl)-2H-pyrazolo[4,3-*b*]pyridin-6-carboxamide (**56**). Prepared from **41** with 1-aminoadamantane and purified by flash chromatography (ethyl acetate/petroleum ether, 2:1) followed by trituration with petroleum ether; yield, 28%; white solid; mp 133-135 °C. ^1H -NMR (400 MHz, CDCl_3) δ : 18.67 and 17.77 (s, 1H), 11.18 and 10.25 (s, 1H), 7.34 and 7.19 (s, 1H), 4.33 (m, 2H), 4.05 (m, 2H), 3.75 (m, 2H), 2.06 (m, 9H), 1.64-1.61 (m, 8H), 0.89 (t, $J = 7.8$ Hz, 3H). ^{13}C -NMR (100 MHz, CDCl_3): δ 171.3, 169.2, 162.4, 132.1, 128.4, 114.8, 96.6, 61.2, 65.2, 52.5, 46.7, 41.6, 41.5, 36.4, 36.2, 29.4, 20.8, 11.4. HRMS (ESI) m/z calcd for $\text{C}_{22}\text{H}_{30}\text{N}_4\text{O}_4$ $[\text{M}+\text{H}]^+$ 415.2340 found 415.2338.

N-(Adamantan-1-yl)-4-(1-butyl)-4,5-dihydro-7-hydroxy-2-(2-hydroxyethyl)-5-oxo-2H-pyrazolo[4,3-*b*]pyridin-6-carboxamide (**57**). Prepared from **42** with 1-aminoadamantane and purified by trituration with petroleum ether/diethyl ether (1:1); yield, 60%; light pink solid; mp 204-205 °C. ^1H NMR (400 MHz, CDCl_3): δ 18.62 and 17.83 (s, 1H), 10.99 and 10.25 (s, 1H), 7.35 (s, 1H), 4.33-4.31 (m, 2H), 4.07-4.03 (m, 2H), 3.77 (t, $J = 7.6$ Hz, 2H), 2.73 (br s, 1H), 2.07-2.04 (m, 10H), 1.67-1.54 (m, 7H), 1.34-1.25 (m, 2H), 0.87 (t, $J = 7.3$ Hz, 3H). ^{13}C NMR (100 MHz, CDCl_3): δ 171.3, 169.2, 162.4, 132.1, 128.4, 114.8, 96.6, 61.2, 56.2, 52.5, 45.0, 41.5, 36.4, 29.6, 29.4, 20.3, 13.8. HRMS (ESI) m/z calcd for $\text{C}_{23}\text{H}_{32}\text{N}_4\text{O}_4$ $[\text{M}+\text{H}]^+$ 429.2496 found 429.2499.

N-(Adamantan-1-yl)-4,5-dihydro-7-hydroxy-2-(2-hydroxyethyl)-5-oxo-4-(1-pentyl)-2H-pyrazolo[4,3-*b*]pyridin-6-carboxamide (**58**). Prepared from **43** with 1-aminoadamantane; purified by flash chromatography (ethyl acetate/methanol, 50:1) followed by trituration with petroleum ether; yield, 52%; white solid; mp 156-157 °C. ^1H NMR (400 MHz, CDCl_3): δ 18.57 and 17.83 (s, 1H), 11.12 and 10.25 (s, 1H), 7.34 (s, 1H), 4.35-4.33 (m, 2H), 4.07-4.05 (m, 2H), 3.80-3.76 (m, 2H), 2.08-2.05 (m, 10H), 1.65-1.61 (m, 7H), 1.30-1.25 (m, 4H), 0.83 (t, $J = 6.6$ Hz, 3H). ^{13}C NMR (100 MHz,

CDCl₃): δ 204.4, 171.3, 169.2, 162.4, 132.0, 128.3, 114.8, 96.6, 61.2, 56.3, 52.5, 45.2, 41.5, 36.4, 29.4, 29.1, 27.3, 22.4, 13.9. HRMS (ESI) m/z calcd for C₂₄H₃₄N₄O₄ [M+H]⁺ 443.2652 found 443.2649.

4,5-Dihydro-7-hydroxy-N-(1-hydroxyadamantan-3-yl)-2-(2-hydroxyethyl)-5-oxo-4-(1-pentyl)-2H-pyrazolo[4,3-b]pyridin-6-carboxamide (59). Prepared from **43** with 3-aminoadamantan-1-ol; purified by flash chromatography (dichloromethane/methanol, 50:2) followed by trituration with petroleum ether; yield, 55%; light yellow solid; mp 144-147 °C. ¹H NMR (400 MHz, CDCl₃): δ 18.64 and 17.59 (s, 1H), 11.21 and 10.33 (s, 1H), 7.35 (s, 1H), 4.36-4.33 (m, 2H), 4.07-4.04 (m, 2H), 3.80-3.76 (m, 2H), 2.23 (s, 2H), 2.07-1.94 (m, 8H), 1.68-1.46 (m, 7H), 1.27-1.10 (m, 4H), 0.84-0.81 (m, 3H). ¹³C NMR (100 MHz, CDCl₃): δ 171.4, 169.0, 162.3, 131.9, 128.4, 115.0, 96.7, 69.2, 61.1, 56.2, 54.7, 48.9, 45.3, 44.0, 40.2, 34.9, 30.6, 29.1, 27.3, 22.4, 13.9. HRMS (ESI) m/z calcd for C₂₄H₃₄N₄O₅ [M+H]⁺ 459.2602 found 459.2606.

N-(Adamantan-1-yl)-4-(1-butyl)-4,5-dihydro-7-hydroxy-1-(2-hydroxyethyl)-5-oxo-2H-pyrazolo[4,3-b]pyridin-6-carboxamide (60). Prepared from **44** and 1-aminoadamantane, it was purified by trituration with petroleum ether/diethyl ether (2:1); yield, 76%; white solid; mp 96-98 °C. ¹H NMR (400 MHz, CDCl₃): δ 18.75 and 18.43 (s, 1H), 10.90 and 10.49 (s, 1H), 7.43 and 7.40 (s, 1H), 4.81-4.68 (m, 2H), 3.99-3.89 (m, 4H), 2.44 (br s, 1H), 2.07 (s, 8H), 1.65 (s, 7H), 1.37-1.31 (m, 4H), 0.88 (t, J = 7.3 Hz, 3H). ¹³C NMR (100 MHz, CDCl₃): δ 171.6, 171.5, 169.2, 166.2, 166.0, 162.0, 130.3, 127.9, 123.8, 123.6, 121.6, 95.4, 92.6, 62.5, 62.1, 53.9, 53.8, 53.3, 52.8, 44.5, 44.3, 41.5, 41.4, 36.3, 36.2, 30.2, 30.1, 29.4, 20.2, 20.0, 13.7, 13.6. HRMS (ESI) m/z calcd for C₂₃H₃₂N₄O₄ [M+H]⁺ 429.2496 found 429.2495.

N-(Adamantan-1-yl)-4,5-dihydro-7-hydroxy-4-(4-hydroxy-1-butyl)-2-methyl-5-oxo-2H-pyrazolo[4,3-b]pyridin-6-carboxamide (61). A suspension of **50** (270 mg, 0.6 mmol) in 10% NaOH solution (6 mL, 1.5 mmol) was refluxed for 1 h. After cooling, the suspension was brought to pH 1 with 4 N HCl and extracted with ethyl acetate. The organic layer was washed with water, dried over anhydrous sodium sulfate, and evaporated. The crude residue was purified by flash chromatography

on silica gel, eluting with dichloromethane/methanol (10:1) to afford **61** (144 mg, 58%) as an oily compound that on treatment with dichloromethane and diethyl ether became a glassy solid. ¹H NMR (400 MHz, CDCl₃): δ 18.56 (s, 1H), 10.17 (br s, 1H), 7.29 (s, 1H), 4.01 (s, 3H), 3.90-3.87 (t, *J* = 7.3 Hz, 2H), 3.66-3.63 (m, 2H), 2.07-1.96 (m, 11H), 1.76-1.73 (m, 2H), 1.64 (m, 6H), 1.60-1.57 (m, 2H). ¹³C NMR (100 MHz, CDCl₃): δ 171.3, 169.4, 162.7, 132.1, 128.7, 114.5, 96.7, 62.3, 52.5, 44.9, 41.5, 40.6, 36.4, 36.2, 29.4, 24.2. HRMS (ESI) *m/z* calcd for C₂₂H₃₀N₄O₄ [M+H]⁺ 415.2340 found 415.2338.

2-(2-Acetoxyethyl)-N-(adamantan-1-yl)-4,5-dihydro-7-hydroxy-5-oxo-4-(1-propyl)-2H-pyrazolo[4,3-b]pyridin-6-carboxamide (62). To an ice-cooled solution of **56** (103 mg, 0.25 mmol) in dry dichloromethane (10 mL) were added dropwise triethylamine (42 μL, 0.3 mmol) and acetyl chloride (18 μL, 0.3 mmol). After stirring at rt for 2 h, a further amount of both triethylamine and acetyl chloride were gradually added and stirring was continued for 30 min. The solution was washed with 1 N HCl, then 5% sodium hydrogen carbonate solution, dried over anhydrous sodium sulfate, and evaporated to dryness. The crude residue was purified by flash chromatography (ethyl acetate/petroleum ether, 2:1, as eluent) to give pure **62** (48 mg, 43%) as a white solid; mp 168-169 °C. ¹H NMR (400 MHz, CDCl₃): δ 17.81 (s, 1H), 10.21 (s, 1H), 7.30 (s, 1H), 4.45 (s, 4H), 3.80 (m, 2H), 2.08-2.05 (m, 9H), 1.94 (s, 3H), 1.70-1.65 (m, 8H), 0.91 (t, *J* = 6.6 Hz, 3H). ¹³C NMR (100 MHz, CDCl₃): δ 171.3, 170.4, 169.4, 162.7, 132.7, 128.7, 114.0, 97.0, 62.5, 52.6, 52.5, 46.8, 41.7, 36.4, 29.4, 29.0, 20.9, 20.7, 11.4. HRMS (ESI) *m/z* calcd for C₂₄H₃₂N₄O₅ [M+H]⁺ 457.2445 found 457.2443.

In Vitro Pharmacological Evaluation. Competition Binding Assay. Membranes from HEK-293 cells over-expressing the respective human recombinant CB1R (*B*_{max} = 2.5 pmol/mg protein) and human recombinant CB2R (*B*_{max} = 4.7 pmol/mg protein) were incubated with [³H]-CP-55,940 (0.14 nM/*K*_d = 0.18 nM and 0.084 nM/*K*_d = 0.31 nM, respectively, for CB1R and CB2R) as the high affinity ligand. Competition curves were performed by displacing [³H]-CP-55,940 with increasing concentration of compounds (0.1 nM – 10 μM). Nonspecific binding was defined by 10 μM of

WIN55,212-2 as the heterologous competitor (K_i values 9.2 nM and 2.1 nM, respectively, for CB1R and CB2R). IC_{50} values were determined for compounds showing >50% displacement at 10 μ M. All compounds were tested following the procedure described by the manufacturer (Perkin Elmer, Italy). Displacement curves were generated by incubating drugs with [3 H]-CP-55,940 for 90 min at 30 $^{\circ}$ C. K_i values were calculated by applying the Cheng-Prusoff equation to the IC_{50} values (obtained by GraphPad) for the displacement of the bound radioligand by increasing concentrations of the test compound. Data represent mean values for at least three independent experiments performed in duplicate and are expressed as the average of K_i (nM) \pm standard deviation.

Functional Activity at CB2R in Vitro. The cAMP HunterTM assay enzyme fragment complementation chemiluminescent detection kit was used to characterize the functional activity in CB2 receptor-expressing cell lines. Gi-coupled cAMP modulation was measured following the manufacturer's protocol (DiscoverX, Fremont, CA). Briefly, CHO-K1 cells overexpressing the human CB2R were plated into a 96 well plate (30,000 cells/well), and incubated overnight at 37 $^{\circ}$ C, 5% CO₂. Media was aspirated and replaced with 30 μ L of assay buffer. Cells were incubated 30 min at 37 $^{\circ}$ C with 15 μ L of 3x dose-response solutions of samples prepared in presence of cell assay buffer containing a 3x of 25 μ M NKH-477 solution (a water soluble analogue of Forskolin) to stimulate adenylylase and enhance basal cAMP levels. For those compounds showing an increase of cAMP levels, we further investigated their effect upon receptor activation by testing compounds in the presence of JWH-133 selective agonist. Cells were pre-incubated with samples (15 min at 37 $^{\circ}$ C at 6x the final desired concentration) followed by 30 min incubation with JWH-133 agonist challenge at the EC₈₀ concentration (EC₈₀ = 4 μ M, previously determined in separate experiments) in presence of NKH-477 to stimulate adenylylase and enhance cAMP levels. For all protocols, following stimulation, cell lysis and cAMP detection were performed as per the manufacturer's protocol. Luminescence measurements were measured using a GloMax Multi Detection System (Promega, Italy). Data are reported as mean \pm SEM of three independent experiments conducted in triplicate and were normalized considering the NKH-477 stimulus alone as 100% of the response. The percentage of

response was calculated using the following formula: % RESPONSE = 100% x (1– (RLU of test sample – RLU of NKH-477 positive control) / (RLU of vehicle – RLU of NKH-477 positive control)).

For those experiments where compounds were tested in presence of an EC₈₀ CB₂-ligand challenge, the percentage of response was calculated using the following formula: % RESPONSE = 100% x (RLU of sample – RLU of EC₈₀ control) / (RLU of NKH-477 positive control - RLU of EC₈₀ control).

Data were analyzed using PRISM.7 software (GraphPad Software Inc, San Diego, CA).

Cytotoxicity and Cytocompatibility Assays. *Materials.* Normal Human Articular Chondrocytes (NHAC-kn) and chondrocytes growth medium were supplied by Lonza (Switzerland). Fibroblasts NIH3T3, DMEM, trypsin solution, and all the reagents and solvents used for cell culture were purchased by Sigma Aldrich (Germany).

Evaluation of in Vitro Cytotoxicity and Cytocompatibility. In order to evaluate the in vitro cytotoxicity of new products, the direct contact test, proposed by ISO 10995-5, was used.⁴⁴ This test is suitable for sample with various shapes, sizes or physical status (i.e. liquid or solid). The evaluation of in vitro acute toxicity does not depend on the final use for which the product is intended, and the document ISO 10995-5:2009 recommends many cell lines from American Type Collection. Among them, to test the samples cytotoxicity, NIH3T3 mouse fibroblasts were chosen.

Cells for cytocompatibility tests are usually chosen according to the end-use of the products under investigation. In order to evaluate the use of the compound **51** in the treatment of osteoarthritis, Normal Human Chondrocytes derived from normal human articular cartilage were selected. Fibroblasts NIH3T3 and NHAC-kn were propagated in Dulbecco's Modified Eagle's Medium (DMEM) supplemented with 10% fetal calf serum (FCS), 1% L-glutamine and 1% penicillin, and in chondrocytes growth medium. Once at confluence, the cells were washed with PBS 0.1 M, separated with trypsin-EDTA solution and centrifuged at 1000 r.p.m. for 5 min. The pellet was re-suspended in complete medium (dilution 1:15).

Cells (1.5 x 10⁴) suspended in 1 mL of complete medium were seeded in each well of a 24 well round multidish and incubated at 37 °C in 5% CO₂ for 24 h. Then, the culture medium was discharged and

each test compound was added to each well in order to test the following concentrations: 2.5, 7.5, 12.5, 25, 37.5, and 50 μ M. After 24 h of incubation at 37 °C in 5% CO₂, cell viability was determined by Neutral Red Uptake test. The assay was carried out three times in three replicates for each tested concentration. Complete medium was used as negative control.

Chondrocytes proliferation in contact with compound **51** as a function of incubation time (1, 7, and 14 days) was evaluated testing the highest not toxic concentration, 7.5 μ M, using the procedure described above. At any interval (1, 7, and 14 days), cell viability was evaluated by Neutral Red uptake. The assay was carried out three times in three replicates for each incubation time. Complete medium was used as negative control. First of all, the following solutions were prepared in order to determine the percentage of viable cells:

1. Neutral Red (NR) stock solution: 0.33 g NR dye powder in 100 mL sterile H₂O
2. NR medium: 1.0 mL NR stock solution+99.0 routine culture medium pre-warmed to 37 °C
3. NR desorb solution: 1% glacial acetic acid solution + 50% ethanol + 49% H₂O.

At the end of incubation, the routine culture medium was removed from each plate and the cells were carefully rinsed with 1 mL pre-warmed D-PBS 0.1 M. Plates were then gently blotted with paper towels. One millilitre NR medium was added to each dish and further incubated at 37 °C, 95% humidity, 5.0% CO₂ for 3 h. The cells were checked during incubation for NR crystal formation. After incubation, the NR medium was removed and the cells were carefully rinsed with 1 mL pre-warmed D-PBS 0.1 M. PBS was decanted and blotted from the dishes and exactly 1 mL NR desorb solution was added to each sample. Plates were placed on a shaker for 20-45 min to extract NR from the cells and form a homogeneous solution. During this step the samples were covered to protect them from light. Five min after removal from the shaker, absorbance was read at 540 nm with a UV/visible spectrophotometer (Ultraspec 200, Pharmacia Biotech).

Determination of Sulfated Glycosaminoglycans (S-GAG) and Hydroxyproline (HYP) Content. The quantification of S-GAG was determined according to the methods of Farndale *et al.*⁴⁵ by the following procedure. At any interval (1, 7, 14 days of incubation), the culture supernatants were

collected and the samples were treated overnight with 25 U/mL proteinase K at 56 °C. After the inactivation of the enzyme, performed at 90 °C for 10 min, the suspensions were pooled with their respective supernatants and centrifuged at 4000g for 10 min at room temperature. The supernatant was then collected, filtered by 0.1 µm pore size syringe filter and centrifuged at 12000g for 4 min at room temperature. One millilitre of a 1,9-dimethyl-methylene blue solution (DMMB) was added to 100 µL of the filtered supernatant and mixed in order to allow the formation of DMMB-S-GAG complexes in each sample. The complexes were then centrifuged at 12000g for 10 min at room temperature, and the pellet suspended in decomplexation solution. After 30 min of shaking at room temperature, the absorbance of the solutions was spectrophotometrically read at 656 nm by an UV/visible spectrophotometer (Ultraspec200, Pharmacia Biotech). The amounts of S-GAG was determined by using a standard curve obtained with chondroitin-sulfated sodium salt from shark cartilage.

The quantification of HYP in human chondrocytes in contact with compound **51** performed by the HYP assay kit (Sigma-Aldrich, Germany). Briefly, adhered HC were hydrolysed in 100 µL of water and transferred to a pressure-tight vial with PTFE-lined cap. Then, 100 µL of concentrated hydrochloric acid (HCl, 12 M), were added and the samples were hydrolyzed at 120 °C for 3 h. Ten microlitre of supernatant were transferred to a 96 well plates. Then 100 µL of the Chloramine T/Oxidation buffer mixture was added to each sample and standard well and incubated at room temperature for 5 min. At last, 100 µL of the diluted DMAB reagent was added to each well, incubated for 90 min at room temperature and the absorbance was read at 560 nm.

Physicochemical Characterization. *Determination of Kinetic Solubility.* Kinetic solubility at pH 1.0 and pH 7.4 for compounds **45-62** was determined starting from freshly prepared 10 mM DMSO stock solutions. In a 96-well plate, 2 µL of stock solution were added to 198 µL of (i) HCl 0.1 M pH 1.0 or (ii) 10 mM Phosphate Buffered Saline (PBS) buffer pH 7.4, both adjusted to 0.15 M ionic strength by KCl addition. The plate was stirred (250 rpm, 4 h, room temperature). At the end of the incubation time, the precipitated compound was separated by centrifugation (1000 g, 3 min, 20 °C) and an aliquot

of the supernatant was diluted 1:100 with MeOH and injected in the HPLC-UV system for quantification. Calibration curves for each compound were built in MeOH. A Phenomenex Jupiter C18 column (150X4.6 mm; 5 μ m particle size; Phenomenex Inc., USA) with gradient elution was employed for compound separation. Eluent A: water; eluent B: acetonitrile both added of 0.1% v/v HCOOH. A typical gradient was as follows: t = 0 min: A: 20%; B: 80%; t = 10 min: A: 5%; B: 95%; t = 12 min: A: 5%; B: 95%; t = 12.5 min: A: 20%; B: 80%, followed by a 3-min reconditioning time. HPLC flow was 1000 μ L/min. A Shimadzu HPLC-UV gradient system (Shimadzu Corp., Kyoto, Japan) consisting of two Shimadzu LC-10ADvp modules, a 10 μ L Rheodyne sample injector (Rheodyne LLC, USA), a SPD-10Avp UV-VIS detector was employed for data acquisition. Acquisition wavelength was set at 254 nm. Reported in Table 2 are mean values of four independent experiments together with their Standard Deviations.

Determination of Ionization Constants (pKa) and Lipophilicity (Log P_{oct}). A Sirius T3 automatic titrator (Sirius Analytical Instruments, Forest Row, UK), equipped with a combined microelectrode, a microstirrer, a temperature probe, an UV-VIS probe and six precision dispensers for titrant and cosolvent pipetting, was employed to measure ionization constants (pKa) and lipophilicity (Log P_{oct}) of selected compounds **45-46**, **48**, **51-52**. A UV-metric approach was applied for pKa measurements. Briefly, 7 μ L of a DMSO stock solution of each compound were poured into a 2 mL glass vial where different percentages of MeOH (55-35%) and 0.15 M ionic strength adjusted water were then added. Titrations occurred in the 12.0-2.0 pH range, employing 0.5 M HCl as titrant. The system was kept at 25 \pm 0.5 $^{\circ}$ C and under nitrogen atmosphere throughout the experiments. For each titrant addition, UV-Vis spectra were recorded in the 180-700 nm range and compared to those of control samples containing the same percentages of co-solvents (DMSO and MeOH) and no compound. Target factor analysis (TFA) was applied to rationalize the 3D matrix of absorbance at different wavelength vs. pH (Sirius T3 Refine software package, version: 1.1.3.0), which provided the pKa values at fixed MeOH percentages. Aqueous pKa values were then extrapolated by Yasuda-Shedlovsky model from data at decreasing MeOH percentages. Partition coefficients (Log P) in *n*-octanol/water partition system

1
2
3 were determined by non-linear fitting of the potentiometric titration curves, evaluating the shift
4
5 produced by the different *n*-octanol/water ratios on the aqueous p*K*_a of each compound.³⁸ Reported
6
7 in Table 3 are mean values of three independent experiments together with their Standard Deviations.
8
9

10 **In Vivo Pharmacology.** *Animals.* Male 60 day-old Wistar rats (Charles River, Hamburg, Germany)
11
12 initially weighing 225–250 g, were used for all experiments. Animals were housed 4-6 per cage under
13
14 a standard 12 h/12 h light/dark cycle with food and water available ad libitum. Experiments were
15
16 performed between 7 am and 4 pm in the animal house (conventional maintained in open conditions
17
18 and specified pathogen free [maintained in barrier conditions] standards). The procedures on animals
19
20 were performed following the recommendations of the International Association of Studies on Pain
21
22 and 3R policy. The study was approved by the Local Ethics Committee of the Maj Institute of
23
24 Pharmacology PAS (Cracow, Poland, approval number 1130/2014 and 125/2018).
25
26

27 *OA Induction.* To induce OA-like joint lesions, animals were deeply anaesthetized with 5% isoflurane
28
29 (Baxter, Chicago, USA) in 100% O₂ (3,5 l/min). The skin overlying the right knee joint was shaved
30
31 and wiped with 100% ethanol. 1 mg of monoiodoacetate (MIA; Sigma-Aldrich, Poznan, Poland)
32
33 dissolved in 50 µl of 0.9% NaCl was injected intra-articular (i.a.) into the joint cavity with 30G ½
34
35 0.3x13 mm needle. MIA is a glyceraldehyde-3-phosphate dehydrogenase inhibitor disrupting
36
37 glycolysis in chondrocytes, which in consequence causes cell death, cartilage degeneration and
38
39 subchondral bone alterations.^{46a,b}
40
41
42
43

44 *Treatment Paradigm.* Compound **51** was dissolved in vehicle solution, which contained 85% NaCl,
45
46 5% DMSO, 5% kolliphor, 5% EtOH (Sigma-Aldrich, Germany). Compound **51** was administrated
47
48 intraperitoneally (i.p.) on Days 21 and 28 post-MIA injection at the dose 1 mg/kg alone or prior
49
50 administration of 1 mg/kg of the CB2R antagonist AM630 (Tocris, UK). Doses of compound **51** and
51
52 AM630 were selected on the basis of preliminary experiments (unpublished results). Rats of the
53
54 control group were treated with an equal volume of the vehicle solution. Animals were sacrificed on
55
56 Day 28 after MIA injection.
57
58
59
60

Assessment of Pain-Related Responses. After MIA injection, rats were maintained under standard conditions for 28 consecutive days, during which animal's welfare was carefully monitored. MIA-induced model causes biphasic pain response with chronic phase beginning on Day 12 after OA induction and showing stable pain threshold decrease from day 21 post-MIA injection.⁴⁰ In vivo experiments were performed on Days 21 and 28 post-MIA injection. Before experiments, animals were extensively habituated to handling to minimize, on the test day, stress associated with handling by the experimenter. Tester was blinded to the experimental groups throughout the tests. Two different tests were used to assess pain-related responses.

Pressure Application Measurement Test. The pressure application measurement (PAM) device (Ugo Basile, Italy) has been used for the mechanical stimulation and assessment of joint pain. A detailed description of the experimental procedure is given elsewhere.⁴⁷ Briefly, a quantifiable force was applied for direct stimulation of the joint, and the automatic readout of the response was recorded. The animal was held lightly, and the operator placed a thumb with a force transducer mounted unit (circular contact 8 mm, joint surface area of 50.3mm²) on one side of the animal's knee joint and a forefinger on the other. A gradually increasing squeeze force was applied across the joint at a rate of approximately 300 g/s with a maximum test duration of 15 s. The peak gram force (gf) applied immediately before the limb base unit recorded withdrawal, and this value was designated as the limb withdrawal threshold (LWT). On Days 21 and 28 the basal measurements were performed before and 60, 120, 180, 240, and 300 min post-drug injection. Two measurements of the ipsilateral limb was obtained and the mean LWTs were calculated and converted to per cent of maximum possible effect (% MPE) according to formula $\% \text{ MPE} = (\text{test result} - \text{baseline result} / \text{cut-off result} - \text{baseline result}) \times 100$.

Kinetic Weight Bearing Test. In order to characterize the forces applied on injured paw during mechanical loading and walking pattern in MIA rats the kinetic weight bearing (KWB, Bioseb, France) instrument was used. It consists of 1 m long corridor lined with piezoelectric sensors on the ground measuring weight borne by each individual paw during a walking sequence of a freely moving

animal. Moreover, at the same time built-in camera detects center of gravity of the animal. Rats were trained to move the corridor one week prior the actual experiment. On Days 21 and 28 basal measurements were performed immediately before and 60 min after drug injection. A single KWB measurement was recorded for 6 consecutive min; if an animal failed to make any correct run during this time period, it was excluded from data analysis. Based on the raw data, KWB software's algorithms computed Peak force (cN) parameter as mean of maximum forces of each rear left or right (injured) paw prints.

RNA Isolation and Quantitative Polymerase Chain Reaction (qPCR) on Human Osteoarthritic Chondrocytes Stimulated with TNF α . Human Osteoarthritic Chondrocytes (HC-OA) derived from human articular cartilage of donors with OA (Cell Applications, Inc, USA) were used in the study. HC-OA cells were stimulated with TNF α in a dose 50 ng/mL after 1 h compound **51** (10 μ M) alone or in combination with AM-630 (1 μ M) was added to the media for next 5 h. After stimulation samples were collected in 1 mL of Trizol reagent (Invitrogen, Carlsbad, CA) and frozen at -80°C until RNA isolation. RNA isolation was performed according to the manufacturer's protocol. The total RNA quantity was assessed using a Nanodrop spectrophotometer (ND-1000, Nanodrop; Labtech International, United Kingdom). Each sample was equalized to a concentration of 1 $\mu\text{g}/\mu\text{L}$ and reverse transcribed to cDNA using iScript Reverse Transcription Supermix (BioRad, Valencia, CA, USA) according to the manufacturer's protocol. The qPCR reactions were carried out using SYBR Green MasterMix (BioRad). The reactions were run on a Real-Time PCR CFX96 TouchSystem (Bio-Rad). Expression levels were assessed against housekeeping gene – B2m. Cycle threshold values were calculated automatically by the CFX Manager software. RNA abundance was calculated as $2^{-(\text{threshold cycle})}$.

Statistical Analysis. The analysis was performed using Statistica 10 (StatSoft Poland), graphs were prepared using Prism 5 (GraphPad Software, San Diego, USA). All data are presented as the mean \pm S.E.M. The results of the in vivo experiments were evaluated by the analysis of variance (ANOVA) followed by Tukey post-hoc test (PAM test) and Bonferroni's post-hoc test (KWB test). RT-qPCR

analysis was made by analysis of variance (ANOVA) followed by Dunnet post-hoc test. All *in vivo* experiments were performed on male Wistar rats. Testing groups for KWB were assigned as follows: n = 22 for Vehicle, n = 10 for Compound 51, n = 10 for AM-630 + Compound 51, n = 5 for AM-630. PAM test includes groups as follow n = 17 for Vehicle, n = 10 for Compound 51, n = 10 for AM-630 + Compound 51, n = 6 for AM-630. The RT-qPCR experiments includes 2 -14 samples. All data were considered significant only when $p < 0.05$; ** $p < 0.01$; *** $p < 0.001$, **** $p < 0.0001$. * denotes significant differences *vs* vehicle group (PAM, RT-qPCR) or *vs* rear left paw (KWB). # denotes significant differences between *vs* TNF α group (RT-qPCR) or *vs* compound **51** group (KWB).

ASSOCIATED CONTENT

Supporting Information

The Supporting Information is available free of charge on the ACS Publications website at DOI: xxxxxx.

Figures illustrating X-ray crystallographic data for compounds **4**, **6**, tautomeric equilibrium data for compound **51**, and HPLC-MS traces and elemental analysis of compounds **45-62** (PDF).

Table 1S reporting the estimated physicochemical characteristics of compounds **45-62**.
Molecular formula strings (CSV).

AUTHOR INFORMATION

Corresponding Authors

*CM, E-mail: claudia.mugnaini@unisi.it. Phone: (+39)0577-234318. Fax: (+39)0577-234333.

*AL, E-mail: alessia.ligresti@icb.cnr.it. Phone: (+39)081-5249573. Fax: (+39)081-8675340.

ORCID

Claudia Mugnaini: 0000-0003-1998-732X

Magdalena Kostrzewa: 0000-0002-3395-5191

Marta Bryk: 0000-0002-6980-8273

Ali Mokhtar Mahmoud: 0000-0003-2328

Antonella Brizzi: 0000-0002-2310-9899

Stefania Lamponi: 0000-0002-2788-8797

Gianluca Giorgi: 0000-0002-8817-7745

Francesca Ferlenghi: 0000-0003-1061-1991

Federica Vacondio: 0000-0002-0729-4385

Giancarlo Colombo: 0000-0002-0194-8149

Marco Mor: 0000-0003-0199-1849

Katarzyna Starowicz: 0000-0003-0091-0066

Vincenzo Di Marzo: 0000-0002-1490-3070

Alessia Ligresti: 0000-0003-1787-3900

Federico Corelli: 0000-0002-5750-4504

Author Contributions

[†]C.M. and [†]M.K. joint first authors. The manuscript was written through contributions of all authors.

All authors have given approval to the final version of the manuscript.

Notes

The authors declare no competing financial interest.

ACKNOWLEDGMENTS

KS and MB work was supported by Departmental Statutory funds (Maj Institute of Pharmacology, Polish Academy of Sciences) and by the National Science Centre, Poland, grant OPUS 2014/13/B/NZ7/02311.

AMM and MK are recipients of a scholarship from INCIPIT PhD programme, which is co-funded by the COFUND scheme Marie Skłodowska-Curie Actions (HORIZON 2020/MSCA grant agreement 665403). We thank Mr. Marco Allarà, Endocannabinoid Research Group, for technical help in in vitro assays, Dr. Simone Esposito, Department of DMPK, IRBM, Pomezia (Rome), Italy, for HRMS determinations, and Dr. Elena Dreassi, Dipartimento di Biotecnologie, Chimica e Farmacia, for HPLC-MS analyses. Authors from Dipartimento di Biotecnologie, Chimica e Farmacia acknowledge the partial support by MIUR Progetto *Dipartimenti di Eccellenza 2018-2022*, grant n. L. 232/2016.

ABBREVIATIONS USED

AcCl, acetyl chloride; ANOVA, analysis of variance; CB1R, type-1 cannabinoid receptors; CB2R, type-2 cannabinoid receptors; CLogP, calculated logarithm of the partition coefficient; CNS, central nervous system; DCM, dichloromethane; DMEM, Dulbecco's modified Eagle's medium; DMMB, 1,9-dimethyl-methylene blue; DRG, dorsal root ganglion; HBA, hydrogen bond acceptor; HBD, hydrogen bond donor; HC, human chondrocytes; HC-OA, human osteoarthritic chondrocytes; HYP, hydroxyproline; IL-1 β , interleukin-1 β ; ip, intraperitoneal; KWB, kinetic weight bearing; LLE, lipophilic ligand efficiency; MIA, sodium monoiodoacetate; MPE, maximal possible effect; MW, molecular weight; NHAC-kn, normal human articular chondrocytes; NRU, neutral red uptake; OA, osteoarthritis; PAM, pressure applied measurement; qPCR, quantitative polymerase chain reaction; SAR, structure-activity relationship; SEM, standard error of the mean; SD, standard deviation of the mean; S-GAG, sulfated glycosaminoglycans; SI, selectivity index; TNF α , tumor necrosis factor alpha; TPSA, topological polar surface area.

REFERENCES

1. Cross, M.; Smith, E.; Hoy, D.; Nolte, S.; Ackerman, I.; Fransen, M.; Bridgett, L.; Williams, S.; Guillemin, F.; Hill, C. L.; Laslett, L. L.; Jones, G.; Cicuttini, F.; Osborne, R.; Vos, T.; Buchbinder, R.; Woolf, A.; March, L. The global burden of hip and knee osteoarthritis: estimates from the global burden of disease 2010 study. *Ann. Rheum. Dis.* **2014**, *73*, 1323–1330.
2. Mobasheri, A.; Bay-Jensen, A.-C.; van Spil, W. E.; Larkin, J.; Levesque, M. C. Osteoarthritis year in review 2016: biomarkers (biochemical markers). *Osteoarthritis Cartilage* **2017**, *25*, 199–208.
3. Langley, P.; Müller-Schwefe, G.; Nicolaou, A.; Liedgens, H.; Pergolizzi, J.; Varrassi, G. The impact of pain on labor force participation, absenteeism and presenteeism in the European Union. *J. Med. Econ.* **2010**, *13*, 662–672.
4. Sofat, N.; Ejindu, V.; Kiely, P. What makes osteoarthritis painful? The evidence for local and central pain processing. *Rheumatology* **2011**, *50*, 2157–2165.
5. Berenbaum, F. Osteoarthritis as an inflammatory disease (osteoarthritis is not osteoarthrosis!). *Osteoarthritis Cartilage* **2013**, *21*, 16–21.
6. Neogi, T. The epidemiology and impact of pain in osteoarthritis. *Osteoarthritis Cartilage* **2013**, *21*, 1145–1153.
7. Conaghan, P. G. Osteoarthritis in 2012: parallel evolution of OA phenotypes and therapies. *Nat. Rev. Rheumatol.* **2013**, *9*, 68–70.
8. Barr, A. J.; Campbell, T. M.; Hopkinson, D.; Kingsbury, S. R.; Bowes, M. A.; Conaghan, P. G. A systematic review of the relationship between subchondral bone features, pain and structural pathology in peripheral joint osteoarthritis. *Arthritis Res. Ther.* **2015**, *17*, 228 (36 pages).
9. Fusco, M.; Skaper, S. D.; Coaccioli, S.; Varrassi, G.; Paladini, A. Degenerative joint diseases and neuroinflammation. *Pain Pract.* **2017**, *17*, 522–532.
10. Fei, J.; Liang, B.; Jiang, C.; Ni, H.; Wang, L. Luteolin inhibits IL-1 β -induced inflammation in rat chondrocytes and attenuates osteoarthritis progression in a rat model. *Biomed. Pharmacother.* **2019**, *109*, 1586–1592.
11. Zhang, W.; Ouyang, H.; Dass, C. R.; Xu, J. Current research on pharmacologic and regenerative

- therapies for osteoarthritis. *Bone Res.* **2016**, *4*, 15040 (16 pages); doi:10.1038/boneres.2015.40
12. Mobasheri, A. The future of osteoarthritis therapeutics: targeted pharmacological therapy. *Curr. Rheumatol. Rep.* **2013**, *15*, 364.
13. (a) Matsuda, L. A.; Lolait, S. J.; Brownstein, M. J.; Young, A. C.; Bonner, T. I. Structure of a cannabinoid receptor and functional expression of the cloned cDNA. *Nature* **1990**, *346*, 561–564; (b) Munro, S.; Thomas, K. L.; Abu-Shaar, M. Molecular characterization of a peripheral receptor for cannabinoids. *Nature* **1993**, *365*, 61–65.
14. Makriyannis, A. 2012 Division of medicinal chemistry award address. Trekking the cannabinoid road: A personal perspective. *J. Med. Chem.* **2014**, *57*, 3891–3911.
15. Tam, J.; Trembovler, V.; Di Marzo, V.; Petrosini, S.; Leo, G.; Alexandrovich, A.; Regev, E.; Casap, N.; Shteyer, A.; Ledent, C.; Karsak, M.; Zimmer, A.; Mechoulam, R.; Yirmiya, R.; Shohami, E.; Bab, I. The cannabinoid CB1 receptor regulates bone formation by modulating adrenergic signaling. *FASEB J.* **2008**, *22*, 285–294.
16. Ofek, O.; Karsak, M.; Leclerc, N.; Fogel, M.; Frenkel, B.; Wright, K.; Tam, J.; Attar-Namdar, M.; Kram, V.; Shohami, E.; Mechoulam, R.; Zimmer, A.; Bab, I. Peripheral cannabinoid receptor, CB2, regulates bone mass. *Proc. Natl. Acad. Sci. USA.* **2006**, *103*, 696–701.
17. Wasserman, E.; Tam, J.; Mechoulam, R.; Zimmer, A.; Maor, G.; Bab, I. CB1 cannabinoid receptors mediate endochondral skeletal growth attenuation by Δ^9 -tetrahydrocannabinol. *Ann. N. Y. Acad. Sci.* **2015**, *1335*, 110–119.
18. Gui, H.; Tong, Q.; Qu, W.; Mao, C. M.; Dai, S. M. The endocannabinoid system and its therapeutic implications in rheumatoid arthritis. *Int. Immunopharmacol.* **2015**, *26*, 86–91.
19. Han, S.; Thoresen, L.; Jung, J.-K.; Zhu, X.; Thatte, J.; Solomon, M.; Gaidarov, I.; Unett, D. J.; Yoon, W. H.; Bardern, J.; Sadeque, A.; Usmani, A.; Chen, C.; Semple, G.; Grottick, A. J.; Al-Shamma, H.; Christopher, R.; Jones, R. M. Discovery of APD371: Identification of a highly potent and selective CB₂ agonist for the treatment of chronic pain. *ACS Med. Chem. Lett.* **2017**, *8*, 1309–1313.

20. (a) Aghazadeh Tabrizi, M.; Baraldi, P. G.; Borea, P. A.; Varani, K. Medicinal chemistry, pharmacology, and potential therapeutic benefits of cannabinoid CB₂ receptor agonists. *Chem. Rev.* **2016**, *116*, 519–560; (b) Han, S.; Thatte, J.; Buzard, D. J.; Jones, R. M. Therapeutic utility of cannabinoid receptor type 2 (CB₂) selective agonists. *J. Med. Chem.* **2013**, *56*, 8224–8256.
21. (a) Pasquini, S.; Botta, L.; Semeraro, T.; Mugnaini, C.; Ligresti, A.; Palazzo, E.; Maione, S.; Di Marzo, V.; Corelli, F. Investigations on the 4-quinolone-3-carboxylic acid motif. 2. Synthesis and structure-activity relationship of potent and selective cannabinoid-2 receptor agonists endowed with analgesic activity in vivo. *J. Med. Chem.* **2008**, *51*, 5075–5084. (b) Pasquini, S.; Ligresti, A.; Mugnaini, C.; Semeraro, T.; Cicione, L.; De Rosa, M.; Guida, F.; Luongo, L.; De Chiaro, M.; Cascio, M.G.; Bolognini, D.; Marini, P.; Pertwee, R.; Maione, S.; Di Marzo, V.; Corelli, F. Investigations on the 4-quinolone-3-carboxylic acid motif. 3. Synthesis, structure–affinity relationships, and pharmacological characterization of 6-substituted 4-quinolone-3-carboxamides as highly selective cannabinoid-2 receptor ligands. *J. Med. Chem.* **2010**, *53*, 5915–5928. (c) Pasquini, S.; De Rosa, M.; Pedani, V.; Mugnaini, C.; Guida, F.; Luongo, L.; De Chiaro, M.; Maione, S.; Dragoni, S.; Frosini, M.; Ligresti, A.; Di Marzo, V.; Corelli, F. Investigations on the 4-quinolone-3-carboxylic acid motif. 4. Identification of new potent and selective ligands for the cannabinoid type 2 receptor with diverse substitution patterns and anti-hyperalgesic effects in mice. *J. Med. Chem.* **2011**, *54*, 5444–5453. (d) Mugnaini, C.; Nocerino, S.; Pedani, V.; Pasquini, S.; Tafi, A.; De Chiaro, M.; Bellucci, L.; Valoti, M.; Guida, F.; Luongo, L.; Dragoni, S.; Ligresti, A.; Rosenberg, A.; Bolognini, D.; Cascio, M. G.; Pertwee, R. G.; Moaddel, R.; Maione, S.; Di Marzo, V.; Corelli, F. Investigations on the 4-quinolone-3-carboxylic acid motif. 5. Modulation of the physicochemical profile of a set of potent and selective CB₂ ligands through a bioisosteric approach. *ChemMedChem* **2012**, *7*, 920–934. (e) Pasquini, S.; De Rosa, M.; Ligresti, A.; Mugnaini, C.; Brizzi, A.; Caradonna, N. P.; Cascio, M. G.; Bolognini, D.; Pertwee, R. G.; Di Marzo, V.; Corelli, F. Investigations on the 4-quinolone-3-carboxylic acid motif. 6. Synthesis and pharmacological evaluation of 7-substituted 4-quinolone-3-carboxamide derivatives as high affinity ligands for cannabinoid receptors. *Eur. J. Med. Chem.* **2012**, *58*, 30–43.

22. Annunziata, P.; Cioni, C.; Mugnaini, C.; Corelli, F. Potent immunomodulatory activity of a highly selective cannabinoid CB2 agonist on immune cells from healthy subjects and patients with multiple sclerosis. *J. Neuroimmunol.* **2017**, *303*, 66–74.
23. Contartese, A.; Valoti, M.; Corelli, F.; Pasquini, S.; Mugnaini, C.; Sgaragli, G. P.; Frosini, M. A novel substituted 4-quinolone-3-carboxylic acid derivative CB2 agonist, COR167, potently protects rat brain cortical slices against OGD and reperfusion injury. *Pharmacol. Res.* **2012**, *66*, 555–563.
24. Cascio, M. G.; Bolognini, D.; Pertwee, R. G.; Palazzo, E.; Corelli, F.; Pasquini, S.; Di Marzo, V.; Maione, S. In vitro and in vivo pharmacological characterization of two novel selective cannabinoid CB2 receptor inverse agonists. *Pharmacol. Res.* **2010**, *61*, 349354.
25. Mugnaini, C.; Brizzi, A.; Ligresti, A.; Allarà, M.; Lamponi, S.; Vacondio, F.; Silva, C.; Mor, M.; Di Marzo, V.; Corelli, F. Investigations on the 4-quinolone-3-carboxylic acid motif. 7. Synthesis and pharmacological evaluation of 4-quinolone-3-carboxamides and 4-hydroxy-2-quinolone-3-carboxamides as high affinity cannabinoid receptor 2 (CB2R) ligands with improved aqueous solubility. *J. Med. Chem.* **2016**, *59*, 1052–1067.
26. (a) Jönsson, S.; Andersson, G.; Fex, T.; Fristedt, T.; Hedlung, G.; Jansson, K.; Abramo, L.; Fritzson, I.; Pekarski, O.; Runström, A.; Sandin, H.; Thuvesson, I.; Björk, A. Synthesis and biological evaluation of new 1,2-dihydro-4-hydroxy-2-oxo-3-quinolinecarboxamides for treatment of autoimmune disorders: structure-activity relationship. *J. Med. Chem.* **2004**, *47*, 2075–2088. (b) Jansson, K.; Fristedt, T.; Olsson, A.; Svensson, B.; Jönsson, S. Synthesis and reactivity of laquinimod, a quinoline-3-carboxamide: intramolecular transfer of the enol proton to a nitrogen atom as a plausible mechanism for ketene formation. *J. Org. Chem.* **2006**, *71*, 1658–1667.
27. Aghazadeh Tabrizi, M.; Baraldi, P. G.; Saponaro, G.; Moorman, A. R.; Romagnoli, R.; Preti, D.; Baraldi, S.; Corciulo, C.; Vincenzi, F.; Borea, P. A.; Varani, K. Design, synthesis, and pharmacological properties of new heteroarylpyridine/heteroarylpyrimidine derivatives as CB₂ cannabinoid receptor partial agonists. *J. Med. Chem.* **2013**, *56*, 1098–1112.
28. Aghazadeh Tabrizi, M.; Baraldi, P. G.; Saponaro, G.; Moorman, A. R.; Romagnoli, R.; Preti, D.;

- Baraldi, S.; Ruggiero, E.; Tintori, C.; Tuccinardi, T.; Vincenzi, F.; Borea, P. A.; Varani, K. Discovery of 7-oxopyrazolo[1,5-*a*]pyrimidine-6-carboxamides as potent and selective CB₂ cannabinoid receptor inverse agonists. *J. Med. Chem.* **2013**, *56*, 4482–4496.
29. Jansson, K.; Fristedt, T.; Olsson, A.; Svensson, B.; Jönsson, S. Synthesis and reactivity of laquinimod, a quinoline-3-carboxamide: intramolecular transfer of the enol proton to a nitrogen atom as a plausible mechanism for ketene formation. *J. Org. Chem.* **2006**, *71*, 1658–1667.
30. Rinaldi-Carmona, M.; Barth, F.; Millan, J.; Derocq, J. M.; Casellas, P.; Congy, C.; Oustric, D.; Sarrau, M.; Bouaboula, M.; Calandra, B.; Portier, M.; Shire, D.; Breliere, J. C.; Le Fur, G. L. SR144528, the first potent and selective antagonist of the CB₂ cannabinoid receptor. *J. Pharmacol. Exp. Ther.* **1998**, *284*, 644–650.
31. Gillis, E. P.; Eastman, K. J.; Hill, M. D.; Donnelly, D. J.; Meanwell, N. A. Applications of fluorine in medicinal chemistry. *J. Med. Chem.* **2015**, *58*, 8315–8359.
32. Pettersson, M.; Hou, X.; Kuhn, M.; Wager, T. T.; Kauffman, G. W. Quantitative assessment of the impact of fluorine substitution on P-glycoprotein (P-gp) mediated efflux, permeability, lipophilicity, and metabolic stability. *J. Med. Chem.* **2016**, *59*, 5284–5296.
33. Lipinski, C. A.; Lombardo, F.; Dominy, B. W.; Feeney, P. J. Experimental and computational approaches to estimate solubility and permeability in drug discovery and development settings. *Adv. Drug Deliv. Rev.* **1997**, *23*, 3–25.
34. Veber, D. F.; Johnson, S. R.; Cheng, H.-Y.; Smith, B. R.; Ward, K. W.; Kopple, K. D. Molecular properties that influence the oral bioavailability of drug candidates. *J. Med. Chem.* **2002**, *45*, 2615–2623.
35. Murray, C. W.; Erlanson, D. A.; Hopkins, A. L.; Keserü, G. M.; Leeson, P. D.; Rees, D. C.; Reynolds, C. H.; Richmond, N. J. Validity of ligand efficiency metrics. *ACS Med. Chem. Lett.* **2014**, *5*, 616–618.
36. (a) Barton, P.; Riley, R. J. A new paradigm for navigating compound property related drug attrition. *Drug Discovery Today* **2016**, *21*, 72–81. (b) Leeson, P. D.; Springthorpe, B. The influence

- of drug-like concepts on decision-making in medicinal chemistry. *Nat. Rev. Drug Discovery* **2007**, *6*, 881–890.
37. Hitchcock, S. A.; Pennington, L. D. Structure–brain exposure relationships. *J. Med. Chem.* **2006**, *49*, 7559–7583.
38. Avdeef, A. Assessment of Distribution-pH Profiles. In *Lipophilicity in Drug Action*, Pliska, V.; Testa, B.; Van de Waterbeemd, H., Eds.; VCH: Weinheim, **1995**; pp 109–139.
39. Caron, M. J.; Emans, P. J.; Coolsen, M. M. E.; Voss, L.; Surtel, D. A. M.; Cremers, A.; van Rhijn, L. W.; Welting, T. J. M. Redifferentiation of dedifferentiated human articular chondrocytes: comparison of 2D and 3D cultures. *Osteoarthritis Cartilage* **2012**, *20*, 1170–1178.
40. (a) Malek, N.; Mlost, J.; Kostrzewa, M.; Starowicz, K. New tool to assess walking patterns in the development of OA pain: kinetic weight bearing. *Osteoarthritis Cartilage* **2017**, *25*, S136–S137. (b) Leuchtweis, J.; Imhof, A.-K.; Montechiaro, F.; Schaible, H.-G.; Boettger, M. K. Validation of the digital pressure application measurement (PAM) device for detection of primary mechanical hyperalgesia in rat and mouse antigen-induced knee joint arthritis. *Methods Find. Exp. Clin. Pharmacol.* **2010**, *32*, 575–583. (c) Barton, N. J.; Strickland, i. T.; Bond, S. M.; Brash, H. M.; Bate, S. T.; Wilson, A. W.; Chessell, I. P.; Reeve, A. J.; McQueen, D. S. Pressure application measurement (PAM): A novel behavioural technique for measuring hypersensitivity in a rat model of joint pain. *J. Neurosci. Methods* **2007**, *163*, 67–75.
41. (a) Malek, N.; Mlost, J.; Kostrzewa, M.; Starowicz, K. New tool to assess walking patterns in the development of OA pain: kinetic weight bearing. *Osteoarthritis Cartilage* **2017**, *25*, S136–S137. (b) Leuchtweis, J.; Imhof, A.-K.; Montechiaro, F.; Schaible, H.-G.; Boettger, M. K. Validation of the digital pressure application measurement (PAM) device for detection of primary mechanical hyperalgesia in rat and mouse antigen-induced knee joint arthritis. *Methods Find. Exp. Clin. Pharmacol.* **2010**, *32*, 575–583. (c) Barton, N. J.; Strickland, i. T.; Bond, S. M.; Brash, H. M.; Bate, S. T.; Wilson, A. W.; Chessell, I. P.; Reeve, A. J.; McQueen, D. S. Pressure application measurement

- (PAM): A novel behavioural technique for measuring hypersensitivity in a rat model of joint pain. *J. Neurosci. Methods* **2007**, *163*, 67–75.
42. (a) Kostrzewa, M.; Malek, N.; Pajak, A.; Starowicz, K. Therapeutic Benefits of Targeting CB2 Receptors in the MIA Model of Osteoarthritis. 16th World Congress on Pain, Yokohama, Japan, Sep 26–30 2016, Poster Number PTH120. (b) Pajak, A.; Kostrzewa, M.; Malek, N.; Korostynski, M.; Starowicz, K. Expression of matrix metalloproteinases and components of the endocannabinoid system in the knee joint are associated with biphasic pain progression in a rat model of osteoarthritis. *J. Pain Res.* **2017**, *10*, 1973–1989.
43. Aldrich, C.; Bertozzi, C.; Georg, G. I.; Kiessling, L.; Lindsley, C.; Liotta, D.; Merz, K. M., Jr.; Schepartz, A.; Wang, S. The ecstasy and agony of assay interference compounds. *J. Med. Chem.* **2017**, *60*, 2165–2168.
44. Regiec, A.; Mastalarz, H.; Mastalarz, A.; Kochel, A. Methylation of 4-nitro-3(5)-pyrazolecarboxylic acid. *Tetrahedron Lett.* **2009**, *50*, 2624–2627.
45. ISO 10993-5:2009. Biological Evaluation of Medical Devices - Part 5: Tests for in Vitro Cytotoxicity. [<https://www.iso.org/standard/36406.html>] (accessed Mar, 2020).
46. Farndale, R. W.; Sayers, C. A.; Barrett, A. J. A direct spectrophotometric microassay for sulfated glycosaminoglycans in cartilage cultures. *Connect. Tissue Res.* **1982**, *9*, 247–248.
47. (a) Guingamp, C.; Gegout-Pottie, P.; Philippe, L.; Terlain, B.; Netter, P.; Gillet, P. Monoiodoacetate-induced experimental osteoarthritis: a dose-response study of loss of mobility, morphology, and biochemistry. *Arthritis Rheum.* **1997**, *40*, 1670–1679. (b) Janusz, M. J.; Hookfin, E. B.; Heitmeyer, S. A.; Woessner, J. F.; Freemont, A. J.; Hoyland, J. A.; Brown, K. K.; Hsieh, L. C.; Almstead, N. G.; De, B.; Natchus, M. G.; Pikul, S.; Taiwo, Y. O. Moderation of iodoacetate-induced experimental osteoarthritis in rats by matrix metalloproteinase inhibitors. *Osteoarthritis Cartilage* **2001**, *9*, 751–760.
48. Malek, N.; Mrugala, M.; Makuch, W.; Kolosowska, N.; Przewlocka, B.; Binkowski, M.; Czaja, M.; Morera, E.; Di Marzo, V.; Starowicz, K. A multi-target approach for pain treatment: dual

1
2
3
4
5
6
7
8
9
10
11
12
13
14
15
16
17
18
19
20
21
22
23
24
25
26
27
28
29
30
31
32
33
34
35
36
37
38
39
40
41
42
43
44
45
46
47
48
49
50
51
52
53
54
55
56
57
58
59
60

inhibition of fatty acid amide hydrolase and TRPV1 in a rat model of osteoarthritis. *Pain* **2015**, 156, 890–903.

Table of Contents Graphic

